nature communications

Article

https://doi.org/10.1038/s41467-025-66296-5

Fructose and follistatin potentiate acute MASLD during complete hepatic insulin resistance

Received: 4 December 2024

Accepted: 4 November 2025

Published online: 24 November 2025

Check for updates

Rongya Tao[1], Oliver Stöhr[1], Ozlem Tok[2], Ana Andres-Hernando[3], Wei Qiu[1], Baiyu He[1], Caixia Wang[1], Lars Grøntved[4], Charles Burant[5], Sheng Hui[2], Miguel A. Lanaspa[3], Norbert Stefan[6,7,8], Kyle D. Copps[1] & Morris F. White[1]

MASLD (metabolic-associated steatotic liver disease) and MASH (steatohepatitis) are closely associated with hepatic IR (insulin resistance) and T2D. Regardless, insulin-stimulated hepatic lipogenesis is considered essential for MASLD development, as mouse models of complete hepatic IR become diabetic without MASLD when fed high-fat diets. Challenging this notion, we found that male LDKO mice lacking hepatic insulin receptor substrates acutely developed MASLD if fed a fructose-enriched "MASH diet" (GAN) or high-fructose diet. Fructose potentiated hepatic re-esterification of abundant circulating fatty acids in LDKO mice, evidenced by excess ^{13}C incorporation into the glycerol backbone —but not fatty acid chains—of hepatic triacylglyceride after gavage with [U^{13}C] fructose. Suppressing adipose lipolysis in LDKO mice by inactivating hepatic Fst (Follistatin) prevented acute MASLD, whereas over-expressing Fst in wild-type mouse liver accelerated GAN-promoted MASLD/MASH. Compatibly, higher serum FST levels among Tübingen Diabetes Family Study participants clustered with increased adipose IR and greater hepatic triacylglyceride accumulation.

MASLD (Metabolic-dysfunction associated steatotic liver disease[1]), originally called NAFLD (nonalcoholic fatty liver disease), affects more than one-third of the population, making it one of the most common liver disorders worldwide[2–6]. Excess hepatic TAG (triacylglyceride) that characterizes MASLD accumulates when esterification of FFA (free fatty acid) from uncontrolled adipose lipolysis or hepatic DNL (de novo lipogenesis) exceeds TAG losses from hepatic lipid oxidation, ketogenesis, or secretion of VLDL (very low-density lipoprotein)[7]. When FFA supply overwhelms these pathways, toxic lipid species can exacerbate hepatic IR (insulin resistance), MASLD, and features of MASH (metabolic-dysfunction associated steatohepatitis) including fibrogenesis, mitochondrial dysfunction, and oxidative and endoplasmic reticulum stress[1,8–12]. Genetic variation explains only 10-20% of MASLD/MASH, suggesting that environmental factors, such as dietary composition, might contribute strongly[13–16]. Consumption of a western diet high in fat and sugars promotes obesity, systemic IR, and T2D—and most individuals with obesity develop MASLD[16–24].

Although IR correlates strongly with T2D and MASLD, the role of hepatic IR is incompletely understood[25]. Within hepatocytes, the activated InsR (insulin receptor) phosphorylates Irs1 (insulin receptor

[1]Division of Endocrinology Boston Children's Hospital, Harvard Medical School, Boston, MA, USA. [2]Dept. Molecular Metabolism, Harvard T.H. Chan School of Public Health, 665 Huntington Ave, Boston, MA, USA. [3]Division of Endocrinology, Metabolism & Diabetes, Univ. of Colorado Anschutz School of Medicine, 12801 East 17th Avenue, Aurora, CO, USA. [4]Department of Biochemistry and Molecular Biology, University of Southern Denmark, Odense, Denmark. [5]Section of Metabolism, Endocrinology, and Diabetes, Department of Internal medicine, University of Michigan, Ann Arbor, MI, USA. [6]Department of Internal Medicine IV, Division of Endocrinology, Diabetology and Nephrology, University Hospital Tübingen, Tübingen, Germany. [7]Institute of Diabetes Research and Metabolic Diseases (IDM) of the Helmholtz Center Munich, Tübingen, Germany. [8]German Center for Diabetes Research (DZD), Neuherberg, Germany.
e-mail: morris.white@childrens.harvard.edu

substrate 1) and Irs2, activating the Pi3k→Akt (Phosphoinositide 3-kinase→Protein kinase B) cascade, stimulating mTorc1 signaling while inhibiting nuclear FoxO1 transcriptional regulation[26]. Complete hepatic IR—modeled by hepatic deletion of InsR, Irs1/2 (LDKO mice), or Akt1/2—causes diabetes without fatty liver in mice fed chow or a high fat diet (HFD)[27–29]. Thus, to explain the association between T2D and MASLD, the concept of "selective IR" was advanced, in which insulin fails to suppress hepatic glucose production, but continues to promote hepatic lipogenic pathways[27,30]. Several mechanisms of selective hepatic IR have been proposed, including decreased hepatic Irs2 signaling in combination with persistent Irs1 signaling in lipogenic hepatocytes[31–33]. Some evidence for this mechanism is found in MASLD patients[34,35]. However, rates of hepatic DNL after bolus glucose are reduced in MASLD patients, suggesting that the relative excess of DNL-derived TAG in liver and VLDL of MASLD patients might be driven more by a chronic excess of gluconeogenic substrates than by selectively-retained insulin sensitivity of DNL[36,37].

Defects in pathways affecting the healthy storage of TAG within adipose might explain the association of IR and T2D with MASLD[13,15,38]. Although most patients with MASLD are affected by overweight or obesity, 20–30% are insulin resistant with a normal or lean BMI, suggesting that impaired adipose TAG storage contributes to MASLD[10,13,39–46]. Adipose IR is present early in the natural history of T2D, resulting in uncontrolled lipolysis that increases flux of FFA to the liver[47]. Moreover, an estimated 59% of hepatic TAG in MASLD patients is produced through re-esterification of circulating FFA[48]. Evidence that elevated circulating FFA can drive hepatic TAG formation independent of insulin might partially explain the appearance of pathway-selective hepatic IR[49], supporting a critical role for adipose IR in the development of MASLD[50].

Hepatokines are mechanistically important for propagation of IR from the liver to adipose[51]. Our previous work demonstrates that complete hepatic IR in LDKO mice activates nuclear FoxO1, increasing the expression and secretion of Fst (Follistatin)[52]. Circulating Fst promotes adipose IR and lipolysis, and muscle energy expenditure, which together upregulate HGP and attenuate obesity in LDKO mice fed chow or HFD[52,53]. Two Fst isoforms—membrane-bound Fst288 (human FST317) and circulating Fst315 (human FST344)[54–56]—block the binding of Activin A and B, Mstn/Gdf8 (myostatin), or Gdf11 to ActRIIA/B (Activin type II receptors), inhibiting phosphorylation of Smad2/3 transcription factors[57–59]. Although Fst is expressed in many tissues, circulating Fst315 owes mainly to hepatic Foxo1 activation by a high glucagon/insulin ratio, sepsis or hepatic IR[52,60–63]. A large clinical study found that higher circulating human FST associates with T2D risk; consistently, FST increases human adipose tissue lipolysis in vitro[64]. These results suggest that hepatic FOXO1→FST in people might integrate hepatic IR with MASLD.

The rodent GAN diet (Gubra amylin NASH) is a high-fat/fructose/cholesterol diet empirically formulated to reliably produce hepatosteatotic disease with human MASH-like characteristics within the mouse lifetime[22,65–67]. Whereas LDKO mice fed chow or HFD (high-fat/sucrose diet) remain lean and without hepatic steatosis[52,53], we show herein that LDKO mice fed either the GAN diet or a simple HFruD (high-fructose diet) acutely develop MASLD relative to control mice. Our genetic and metabolic investigations of LDKO mice strongly support that dietary fructose potentiates MASLD during complete hepatic IR by enabling re-esterification of FFA mobilized through Fst-promoted adipose IR and lipolysis. Compatible with this mechanism, we further show that high serum FST clusters with increased adipose IR and hepatic lipid content in highly characterized individuals in the Tübingen Family Diabetes Study pre-disposed to development of metabolic disease.

Results

GAN diet promotes acute MASLD and MASH during complete hepatic IR

To investigate how dietary composition affects hepatic lipid accumulation during complete hepatic IR, LDKO mice ($Irs1^{L/L}$•$Irs2^{L/L}$•Cre^{Alb}) and floxed control mice (Cntr) were fed chow diet (Prolab Isopro RMH 3000) or $HFD^{45\%}$ (Research Diets D12451) beginning at 5 weeks of age. After 14 weeks on diet, LDKO mice fed either chow or $HFD^{45\%}$ had a small healthy-appearing liver, whereas Cntr mice fed $HFD^{45\%}$ developed an enlarged steatotic liver (Supplemental Fig. S1a, b and h, i). Similarly, $HFD^{45\%}$ increased liver TAG content only slightly in LDKO mice, compared to a 2-fold increase in Cntr mice (Supplemental Fig. S1c, j). Hepatic DNL assessed by ^3H_2O labeling of hepatic TAG was significantly lower in LDKO mice than in Cntr mice on either chow or $HFD^{45\%}$ (Supplemental Fig. S1d, k). Serum TAG and FFA concentrations were likewise significantly lower in LDKO mice on both diets (Supplemental Fig. S1e, f and l, m). Importantly, there was no difference in food intake between LDKO and Cntr mice fed either chow or $HFD^{45\%}$ (Supplemental Fig. S1g, n). Thus, complete hepatic IR in LDKO mice restricted development of hepatic steatosis during $HFD^{45\%}$.

We reasoned that $HFD^{45\%}$ might incompletely model processed foods associated with MASLD and T2D in humans. Thus, we fed 5-week-old Cntr and LDKO mice the GAN diet (Research Diets D09100310), containing excess sugar (fructose), fat, and cholesterol—which faithfully recapitulates key histological, transcriptional, and metabolic features of human MASLD[68–70]. Although Cntr and LDKO mice consumed equal amounts of the GAN diet (Supplemental Fig. S2a), body and eWAT (epididymal white adipose tissue) masses were significantly lower in LDKO mice (Fig. 1a–c). This result was consistent with the lower body mass of LDKO mice fed $HFD^{45\%}$; however, LDKO mice fed the GAN diet had enlarged steatotic livers containing more TAG, total cholesterol (TC), and FFA than liver from Cntr mice (Fig. 1d–i). Centrifuged serum from the LDKO mice appeared lipemic and contained more than twice as much TAG as serum from Cntr mice (Supplemental Fig. S2b, c). LDKO mice fed the GAN diet developed severe diabetes, including fasting hyperinsulinemia and hyperglycemia, which was absent in Cntr mice fed GAN diet, or in Cntr and LDKO mice fed chow (Supplemental Fig. S2d, e). The LDKO mice fed GAN diet also displayed more severe glucose intolerance than either Cntr mice fed GAN or LDKO mice fed chow (Supplemental Fig. S2f,g).

Remarkably, Masson trichrome and Sirius Red staining of liver from LDKO mice that consumed GAN diet for only ten weeks revealed advanced fibrosis typical of MASH, which was not observed in Cntr liver (Fig. 1j). By comparison, nearly a year of GAN diet consumption is typically required to produce advanced fibrosis in wild-type mice[66,71–73]. Immunostaining of Gal3 (Galectin-3), a marker of fibrotic and inflammatory MASH[73], was also increased in liver sections from LDKO mice fed the GAN diet for 10 weeks (Fig. 1k). Consistent with acute MASH onset, LDKO mice fed GAN diet had a strikingly short life span (Fig. 1l).

$HFruD^{60\%}$ potentiates MASLD during complete hepatic IR

Fructose models the western diet in pre-clinical investigation of MASLD and MASH[22,67,74,75]. Since the GAN diet is high in fat and cholesterol, as well as fructose, we fed Cntr and LDKO mice a simpler high-fructose diet ($HFruD^{60\%}$) containing 60% fructose by weight without excess fat or cholesterol (Envigo TD.89247; 13 kcal% lard, 67 kcal% fructose)[33,76]. LDKO mice fed $HFruD^{60\%}$ for ten weeks had 17% less body mass and 18% less liver mass than Cntr mice (Fig. 2a–d); however, LDKO mice developed greater hepatosteatosis detected by H&E staining (Fig. 2e). Although LDKO and Cntr mice consumed equal $HFruD^{60\%}$, the LDKO mice displayed severe glucose intolerance (Fig. 2f, g). Moreover, hepatic concentrations of TAG, TC, and FFA were significantly higher in LDKO than in Cntr mice (Fig. 2h–j), which was associated with less eWAT mass and higher serum TAG and FFA levels (Fig. 2k–m). Regardless, unlike LDKO mice fed GAN diet for 10 weeks, fibrosis was not detected in liver sections from LDKO mice fed $HFruD^{60\%}$ (Supplemental Fig. 3a). Thus, we fed 5-week-old Cntr and LDKO mice $HFruD^{60\%}$ for 20 weeks. After 20 weeks on $HFruD^{60\%}$, LDKO mice had lower body and eWAT mass than Cntr mice (Supplemental

https://doi.org/10.1038/s41467-025-66296-5

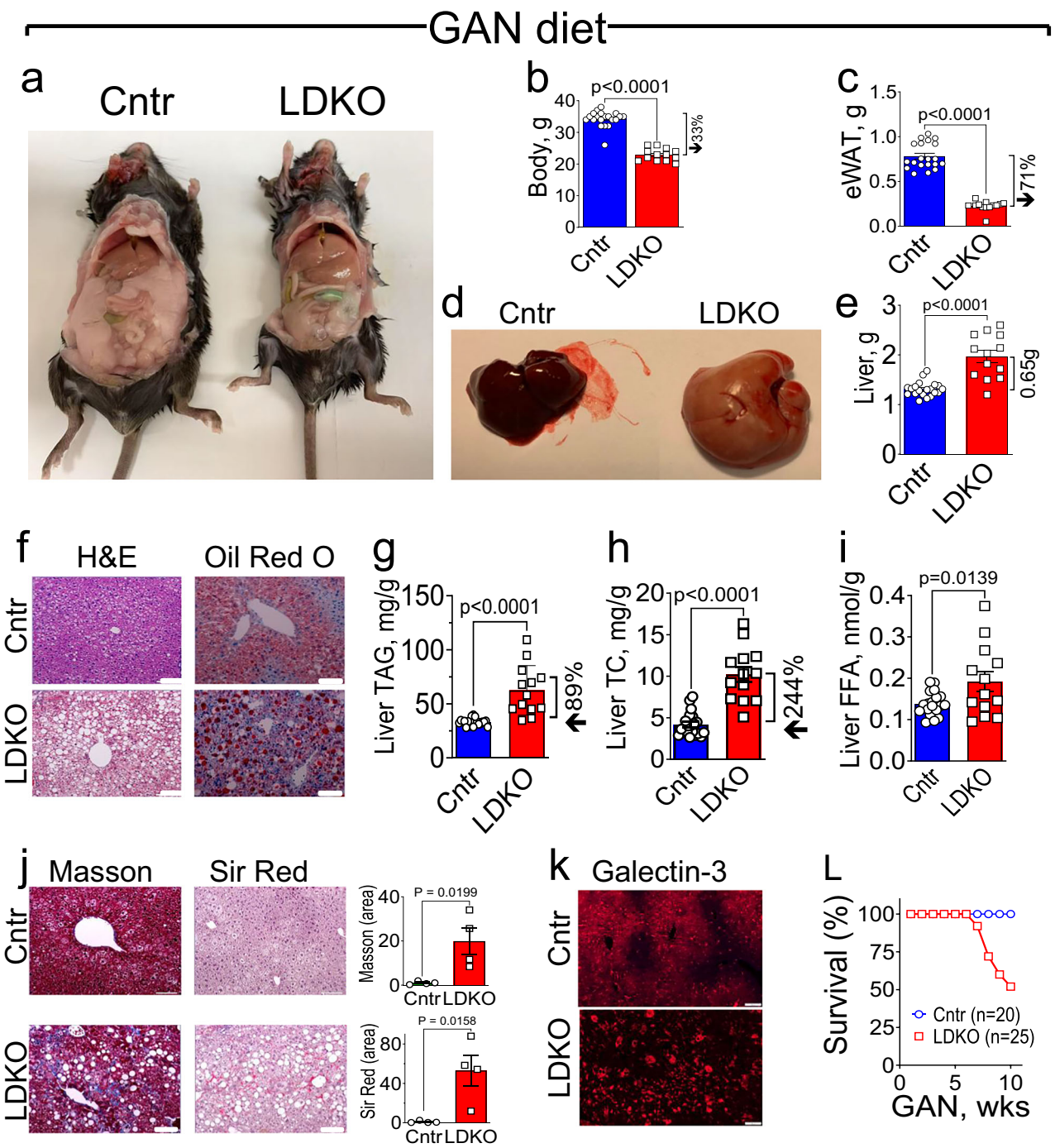

Fig. 1 | GAN diet promotes acute MASLD and MASH during complete hepatic IR. Mice were weaned onto chow at 3 weeks and placed on GAN diet at 5 weeks. **a**–**c** Representative photographs ($n = 3$), body mass ($n = 13, 20$), and eWAT mass ($n = 13, 20$) of 15-week-old Cntr or LDKO mice. **d**, **e** Representative photographs of dissected livers ($n = 3$) and liver masses ($n = 13, 20$) from 15-week-old Cntr or LDKO mice. **f** Representative liver sections stained with H&E or Oil Red O ($n = 4$ mice, scale bar= 100 μm). **g**–**i** TAG, TC, and FFA concentrations determined in the liver extracts ($n = 13, 20$). **j** Representative liver sections stained by Masson or Sir Red and quantified by Image J ($n = 4$ mice, scale bar= 100 μm). **k** Representative liver sections stained by Galectin-3 antibody ($n = 3$ mice, scale bar= 100 μm). **l** Survival of LDKO and Cntr mice fed GAN diet for 10 weeks ($n = 20$–25). Data are means ± SEM. *P* values (**b**, **c**, **e**, and **g**–**j**) were obtained from two-tailed unpaired t-tests. Source data are provided in the Source Data file.

Fig. S3b,c). Liver sections of LDKO mice fed HFruD$^{60\%}$ for 20 weeks appeared similar by H&E staining to those fed HFruD$^{60\%}$ for 10 weeks, and contained a similar excess of TAG relative to Cntr mice (compare Supplemental Fig. S3d, e and Fig. 2e, h); however, LDKO mice fed HFruD$^{60\%}$ for 20 weeks developed adenomatous nodules on the liver surface that were absent in Cntr mice (Supplemental Fig. S3f). Consistent with liver damage, serum ALT was elevated in LDKO mice fed HFruD$^{60\%}$ diet for 20 weeks (Supplemental Fig. S3g); however, hepatic fibrosis was still not detected by Masson or Sirius Red staining (Supplemental Fig. S3h, i). Thus, LDKO mice fed HFruD$^{60\%}$ for a full 20 weeks developed MASLD with liver damage, but without fibrotic MASH. We infer that excess fat and cholesterol in the GAN diet—but omitted from the HFruD$^{60\%}$—are required to accelerate MASLD-to-MASH progression in LDKO mice.

https://doi.org/10.1038/s41467-025-66296-5

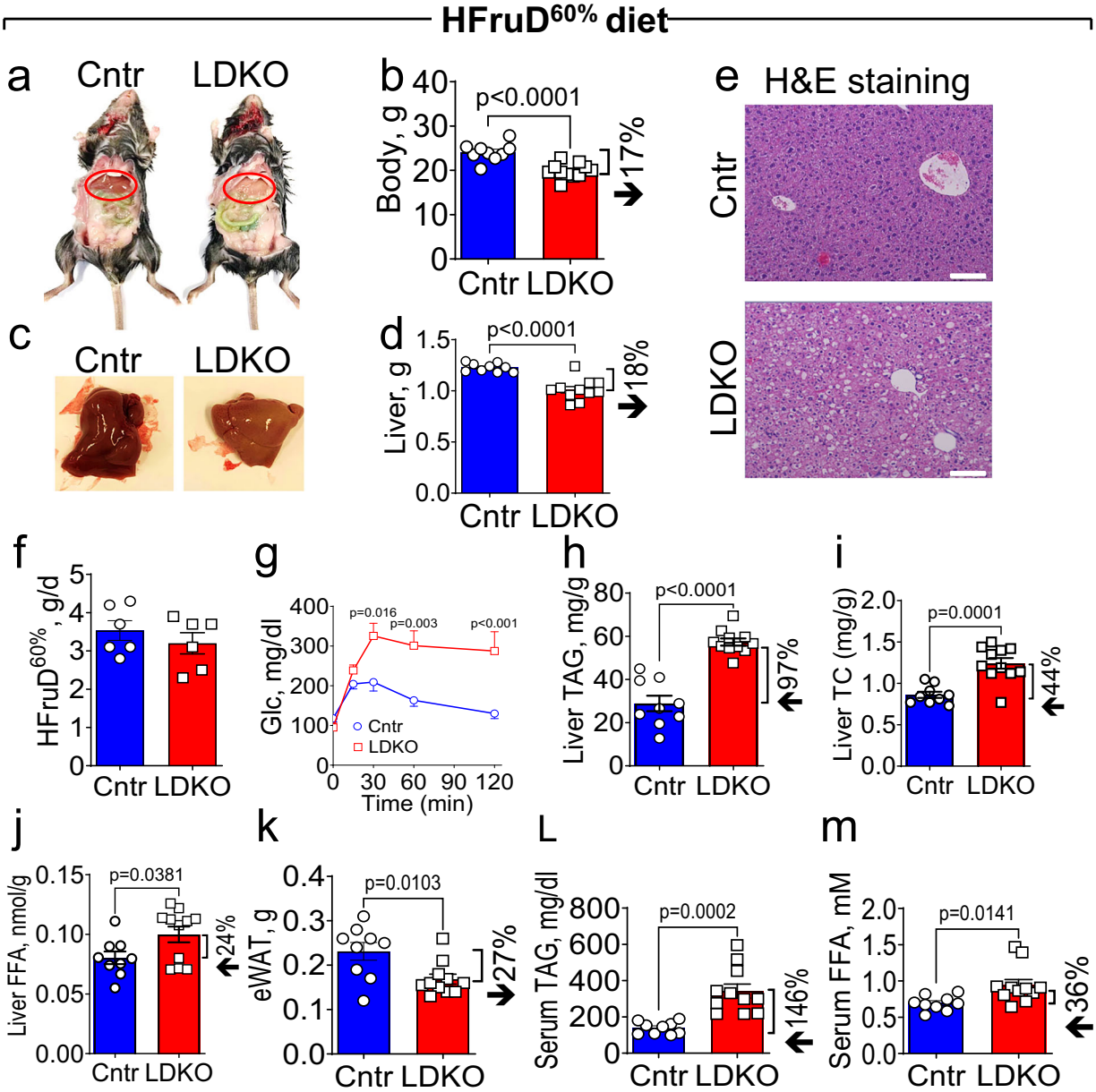

Fig. 2 | HFruD$^{60\%}$ potentiates MASLD during complete hepatic IR. Mice were weaned onto chow at 3 weeks and placed on a HFruD$^{60\%}$ diet at 5 weeks. **a**, **b** Representative photograph ($n = 3$) and body mass ($n = 9, 11$) of 15-week-old Cntr and LDKO mice. **c**–**e** Representative photographs of liver ($n = 3$), liver mass ($n = 9, 11$), and representative H&E-stained liver sections ($n = 4$, scale bar= 100 μm) of 15-week-old Cntr and LDKO mice. **f** HFruD$^{60\%}$ intake by Cntr and LDKO mice ($n = 6$). **g** GTT performed on 11-week-old Cntr and LDKO mice fasted for 6 hrs ($n = 9, 11$). **h**–**j** Concentration of TAG, TC, and FFA in liver extracts ($n = 9, 11$). **k** eWAT mass of 15-week-old Cntr and LDKO mice ($n = 9, 11$). **l**, **m** Serum TAG and FFA levels in 15-week-old Cntr and LDKO mice fasted for 6 hrs ($n = 9, 11$). Data are means ± SEM. *P* values were obtained from (**b**, **d**, and **h**–**j**) two-tailed unpaired t-test or (**g**) two-way ANOVA. Source data are provided in the Source Data file.

Complete hepatic IR exacerbates hepatic inflammation on GAN diet

Inflammation caused by activation of resident Kupffer cells and infiltrating monocytes plays an important role in the progression of MASLD to MASH and its life-threatening sequelae[66,71–73,77,78]. C57BL6 mice fed the GAN diet develop hepatic inflammation between 20-48 weeks and progressive fibrosis with neoplasms that resemble human HCC by 58-68 weeks[22,67]; by contrast, LDKO mice developed fibrotic MASH after only 10 weeks of GAN diet (See Fig. 1j, k). To identify mechanisms engaged during acute MASLD/MASH in LDKO mice, we used RNAseq to assess gene expression in Cntr and LDKO mice fed GAN, HFruD$^{60\%}$, or HFD$^{45\%}$ for 10 weeks. Compared against Cntr mice, iPathway analysis (advaitabio.com) revealed 'NFκB signaling', 'microRNAs in cancer', and 'chemokine signaling' as the top three changed gene sets in liver of LDKO mice fed GAN diet (Supplemental Fig. S4a-c). Nearly all genes in these pathways were upregulated significantly in LDKO liver on the GAN diet. Sets of genes known to be associated with MASLD/MASH also increased significantly in LDKO mice on GAN diet—including TNFα and IL17 signaling, fibrosis (ECM organization), and monocyte recruitment (Supplemental Fig. S4d-g)[66,79]. A subset of these genes increased in LDKO mice fed HFruD$^{60\%}$, whereas few genes differed significantly between Cntr and LDKO mice fed HFD$^{45\%}$ (Supplemental Fig. S4a–g). Thus, genes and pathways associated with fibrotic, inflammatory MASH, and cancer progression were acutely elevated in LDKO mice fed GAN diet, but to a lesser degree by HFruD$^{60\%}$ [66,80].

https://doi.org/10.1038/s41467-025-66296-5

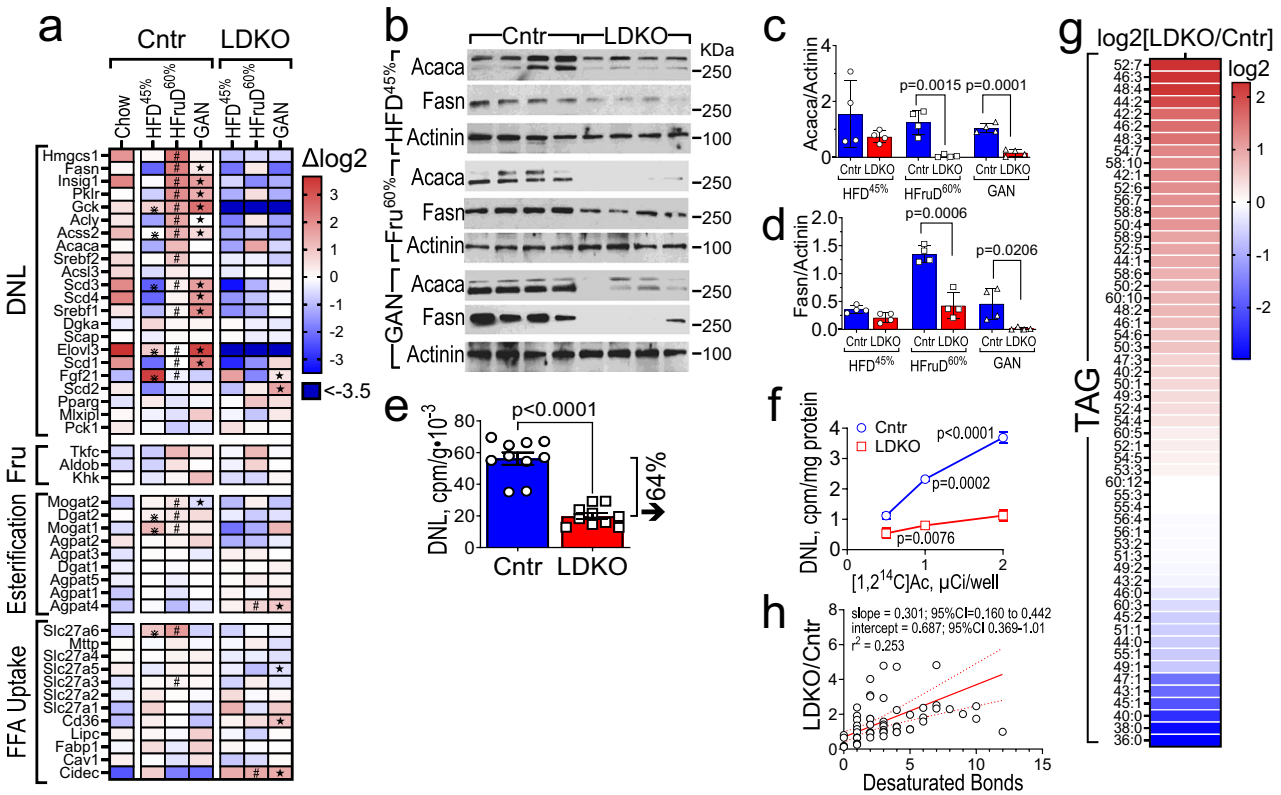

Fig. 3 | The contribution of hepatic DNL to MASLD during complete hepatic IR. Mice were weaned onto chow at 3 weeks and placed on HFD$^{45\%}$, GAN, or HFruD$^{60\%}$ at 5 weeks as indicated. **a** Hepatic expression of genes associated with DNL, fructose metabolism (Fru), lipid esterification, and FFA uptake in 15-week-old Cntr or LDKO mice. Significance (Bonferroni p-value) marks higher gene expression in LDKO or Cntr mice fed GAN (★), HFruD$^{60\%}$ (#), or HFD$^{45\%}$ (✳) ($n = 2$). **b**–**d** Acaca and Fasn protein concentration in liver extracts from 15-week-old Cntr or LDKO mice ($n = 4$). **e** Hepatic DNL measured by $^{3}H_2O$ incorporation in 11-week-old Cntr and LDKO mice fed HFruD$^{60\%}$ ($n = 10$). (f) DNL measured in cultured primary hepatocytes from LDKO and Cntr mice ($n = 3$) by measuring the incorporation of varying doses of [1,2,^{14}C]acetate into lipid. **g** TAG determined by LC–MS in liver extracts from 11-week-old Cntr and LDKO mice fed HFruD$^{60\%}$ ($n = 4$). For each lipid species, the relative estimated means determined by a generalized linear model (SPSS) were ranked by log2[LDKO/Cntr] on a heatmap. **h** Ratios of lipid species (LDKO/Cntr) from (**g**) plotted against the number of desaturated bonds in each lipid detected in liver extracts. The red fitted solid line (± 95% confidence interval, dotted line) was determined in Graphpad Prism using robust regression. Data are means ± SEM. *P* values were obtained from (**c**–**e**) two-tailed unpaired t-test or (**f**) two-way ANOVA. Source data are provided in the Source Data file.

Minimal contribution of hepatic DNL to MASLD during complete hepatic IR

Fatty acids incorporated into hepatic TAG are derived from hepatic DNL, the diet, or adipose lipolysis[48,81]. Fructose promotes hepatic DNL in part by upregulating Chrebp (Carbohydrate-responsive element-binding protein; or MLX-interacting protein-like), Srebp1c (Sterol Regulatory Element Binding Transcription Factor 1), or both[82,83]. We used RNAseq to compare the expression of genes associated with lipogenesis in the liver of Cntr and LDKO mice fed HFD$^{45\%}$, GAN diet, or HFruD$^{60\%}$ for 10 weeks (Fig. 3a). Compatible with attenuated DNL in LDKO mice fed chow or HFD$^{45\%}$ (See Supplemental Fig. S1d,k), the RNA expression of many key mediators of DNL, fatty acid elongation, and desaturation was significantly lower in LDKO mice than in Cntr mice on either GAN or HFruD$^{60\%}$ diets—including Srebp1c (Srebf1), Fasn, Insig1, Pklr, Gck, Acly, Acss2, Elovl3, Scd1 and Scd3 (Fig. 3a). Several of these genes were also expressed at reduced level in LDKO mice fed HFD$^{45\%}$. Consistent with the suppression of DNL, Gck, Acss2, Elovl3, and Scd3 were also reduced in LDKO mice compared to Cntr mice fed the HFD$^{45\%}$ (Fig. 3a)[84]. By contrast, RNA expression of Chrebp (Mlxipl) and fructose metabolic genes—Khk (Ketohexokinase), Aldob (Aldolase B) and Tkfc (Triokinase)—did not differ significantly between Cntr and LDKO mice on any diet (Fig. 3a). Expression of a few genes involved in esterification or uptake of FFA was higher in Cntr than in LDKO mice on at least HFruD$^{60\%}$—including acyltransferases Mogat1, Mogat2, and Dgat2 and fatty acid transporters of the Slc27a family; however, expression of Cidec (Fsp27) was higher in LDKO liver, possibly in aid of hepatic lipid droplet storage in LDKO mice (Fig. 3a). Overall, gene expression related to hepatic DNL and TAG synthesis was generally lower in LDKO than in Cntr mice, particularly on HFruD$^{60\%}$ or GAN diets.

To investigate control of DNL at the protein level, we immunoblotted Acaca (Acetyl CoA carboxylase a) and Fasn (Fatty acid synthase) in liver extracts from mice fed HFD$^{45\%}$, HFruD$^{60\%}$ or GAN (Fig. 3b). Concentrations of both proteins were marginally reduced in LDKO mice fed HFD$^{45\%}$, but strongly reduced in LDKO mice fed HFruD$^{60\%}$ or GAN (Fig. 3b–d). Consistently, hepatic DNL measured by $^{3}H_2O$ incorporation was 64% lower ($p < 0.0001$) in LDKO mice than in Cntr mice fed the HFruD$^{60\%}$ for 10 weeks (Fig. 3e). Fructose can be metabolized by gut microbiota into acetate, which may enter the portal circulation and contribute to hepatic DNL[85]. Regardless, DNL measured using [1,2-^{14}C] acetate tracer was lower in primary hepatocytes from LDKO mice than in Cntr hepatocytes (Fig. 3f).

To infer the origin of fatty acids in hepatic lipid in LDKO or Cntr mice fed HFruD$^{60\%}$, we used LC-MS (liquid chromatography-mass spectrometry). Shotgun lipidomics revealed markedly increased long-chain unsaturated TAGs in LDKO liver (52:7, 48:5, 46:3, 48:4, etc.), but reduced levels of saturated TAGs (44:0, 40:0, 38:0, 36:0, etc.) (Fig. 3g,h). Because DNL generates saturated fatty acid chains[86], these results supported that MASLD in LDKO mice fed HFruD$^{60\%}$ or GAN might owe mostly to hepatic re-esterification of circulating FFA, rather than to hepatic DNL[19,86].

Hepatic Ketohexokinase-C (Khk-C) is not required for acute MASLD/MASH in LDKO mice fed GAN diet

Phosphorylation of fructose by high-activity Khk-C in the liver, intestine or kidney yields F1P (fructose-1-phosphate) that can be cleaved by Aldob to produce GA (glyceraldehyde) and DHAP (dihydroxyacetone phosphate)[87]. To determine whether hepatic fructose phosphorylation was required for diabetes and acute MASLD/MASH in LDKO mice fed the GAN diet, we deleted *Khk* in hepatocytes of LDKO mice, generating LDKO^{KhkKO} mice (Supplemental Fig. S5a). Compared to Cntr mice, body mass in LDKO^{KhkKO} mice fed GAN for 10 weeks was 27% lower ($p < 0.0001$), which was similar to the 33% reduction seen in LDKO mice on GAN (compare Supplemental Fig. S5b, c to Fig. 1a,b, above). Relative to Cntr mice, LDKO^{KhkKO} mice developed fasting hyperglycemia and severe glucose intolerance similar to LDKO mice on GAN diet (compare Supplemental Fig. S5d,e to Fig. S2e–g above). Like LDKO mice on the GAN diet, LDKO^{KhkKO} mice had 64% less eWAT mass than Cntr mice (compare Supplemental Fig. S5f to Fig. 1c, above). Moreover, LDKO^{KhkKO} mice developed severe dyslipidemia—including elevated serum TAG, TC, and FFA levels comparable to those in LDKO mice fed the GAN diet (compare Supplemental Fig. S5g–j to Fig. S2b,c, above). Liver size and mass in LDKO^{KhkKO} mice fed the GAN diet increased 31%, as the liver accumulated more lipid droplets and higher concentrations of TAG and FFA than livers of Cntr mice (Supplemental Fig. S5k–o); however, liver TC was unchanged in LDKO^{KhkKO} compared to Cntr mice, whereas it increased 244% in LDKO compared to Cntr mice fed GAN (compare Fig. S5p to Fig. 1h, above). Thus, only liver TC in LDKO mice fed GAN diet depended upon hepatic Khk-C, whereas diabetes, dyslipidemia, and acute MASLD were independent of hepatic Khk-C.

Fructose potentiates hepatic esterification of FFA in LDKO mice

To investigate how dietary fructose promotes MASLD in LDKO mice, we used LC-MS to quantify polar metabolites in livers of Cntr and LDKO mice that were fed HFruD$^{60\%}$ for 6 weeks, beginning at 5 weeks of age. Compared to Cntr liver, the abundance of 11 different metabolites was significantly lower in LDKO liver (Fig. 4A). Among these, lower glucose-6-phosphate (G6P) was consistent with reduced hepatic Gck (glucokinase) expression in LDKO mice on all diets previously tested (see Fig. 3A above). The abundance of six other metabolites was significantly elevated in LDKO liver, including β-hydroxybutyrate (3-HB) and glycerol-3-phosphate (Gro3P) (Fig. 4A). Higher hepatic 3-HB, which is derived from partially oxidized FFA in mitochondria, was compatible with previously described ketosis and excess urinary ketone output in LDKO mice[52]. Hepatic Gro3P is derived from multiple pathways, including phosphorylation of glycerol from the portal circulation, glycolytic and gluconeogenic pathways, and from reduction of DHAP generated through intrahepatic fructolysis. Since Gro3P is required for synthesis of new hepatic TAG, we confirmed by separate enzymatic assay that hepatic Gro3P increased significantly 2.5-fold in LDKO mice than in Cntr mice fed HFruD$^{60\%}$ for 6 weeks (Fig. 4b).

We hypothesized that increased hepatic Gro3P might enhance re-esterification of excess FFA in livers of LDKO mice fed GAN or HFruD$^{60\%}$ (see Fig. 1i and Fig. 2j, above). To investigate, we analyzed newly formed hepatic TAG from 11-week-old Cntr and LDKO mice that had been maintained on HFruD$^{60\%}$ for 6 weeks. Following a 6 h fast, the mice were gavaged with 2 g/kg [U-^{13}C6] fructose (Fig. 4c). After a two h labeling period, we extracted and saponified hepatic TAG and analyzed both FFA and glycerol fractions by LC-MS (Fig. 4d). Labeling of the FFA fraction (16:0) was never detected in hepatic TAG from Cntr or LDKO mice (Fig. 4e). In contrast, [^{13}C]glycerol—including fully-labeled C3-glycerol, and partly labeled C2- and C1-glycerol—was greater in hepatic TAG from LDKO than Cntr mice (Fig. 4f). Given that DNL was reduced 64% in LDKO mice versus Cntr mice fed HFruD$^{60\%}$ (see Fig. 3e, above), these results suggested that dietary fructose potentiates acute MASLD in LDKO mice mainly by enabling hepatic re-esterification of abundant circulating FFA.

Primary adipose IR promotes hepatic steatosis during GAN diet

Esterification of circulating FFA released through adipose lipolysis contributes significantly to intrahepatic TAG accumulation in MASLD patients[48,81]. In LDKO mice, FoxO1 induces hepatic Fst expression and secretion, promoting adipose IR and lipolysis[52,53]. Thus, serum FFA was 41% higher in LDKO mice than in Cntr mice fed the GAN diet, and injected insulin failed to suppress FFA into the normal range (Supplemental Fig. S6a, b). Consistent with increased delivery of FFA to the LDKO liver, urinary ketones were significantly elevated in LDKO mice fed the GAN diet (Supplemental Fig. S6c).

To investigate the role of adipose IR in MASLD during GAN diet, we used adiponectin-Cre to delete Irs1 and Irs2 in adipose tissues, generating FDKO mice (Irs1$^{L/L}$•Irs2$^{L/L}$•Cre^{Adipoq})[52]. FDKO and Cntr mice fed the GAN diet for 20 weeks had similar body mass, circulating insulin, and glucose tolerance; however, serum FFA was 51% higher in FDKO mice (Supplemental Fig. S7a–d). Consistent with increased hepatic FFA re-esterification, FDKO mice had greater liver mass (↑67%) and hepatic TAG (↑43%) than Cntr mice, whereas eWAT mass decreased 43% (Supplemental Fig. S7e–i). Liver sections from FDKO mice displayed more lipid droplets but no evidence of fibrosis when the experiment was terminated at 25 weeks (Supplemental Fig. S7j,k). Thus, primary/genetic adipose IR in FDKO mice augmented redistribution of lipid from adipose to the liver. These results suggested that Fst-promoted adipose IR and lipolysis are mechanistically important for acute MASLD in LDKO mice fed GAN or HFruD$^{60\%}$.

Hepatic FoxO1→Fst is required for acute MASLD/MASH in LDKO mice fed HFruD$^{60\%}$ or GAN

To establish whether hepatic FoxO1 promotes acute MASLD in LDKO mice, we deleted hepatic FoxO1 in LDKO mice, generating LTKO mice (LDKO•FoxO1$^{L/L}$). LTKO and littermate Cntr3 mice (Irs1$^{L/L}$•Irs2$^{L/L}$•FoxO1$^{L/L}$) were fed HFruD$^{60\%}$ for 10 weeks. Unlike LDKO mice fed HFruD$^{60\%}$ diet for 10 weeks (See Fig. 2a–e, above), the livers from LTKO mice had a normal mass, were non-steatotic, and contained 31% less TAG than livers from Cntr3 mice (Fig. 5a–c). Thus, acute MASLD in LDKO mice fed HFruD$^{60\%}$ required hepatic FoxO1.

Next, we fed LTKO and Cntr3 mice GAN diet for 10 weeks. The body mass of LTKO mice was 12% less than Cntr3 mice (Fig. 5d). Unlike LDKO mice, LTKO mice fed GAN diet did not display excess serum lipid (Fig. 5e). Consistently, liver mass, lipid droplets in H&E sections, and hepatic TAG content were lower than in Cntr3 mice fed GAN diet (Fig. 5f-i). Moreover, Galectin-3 staining was normal and fibrosis was not detected by Masson or Sirius Red staining in sections from LTKO mice (Fig. 5j, k). Thus, hepatic FoxO1 was required for acute MASLD/MASH in LDKO mice fed the GAN diet.

Hepatic Fst mRNA and serum Fst levels were significantly higher in LDKO mice, regardless of the diet (HFD$^{45\%}$, HFruD$^{60\%}$, or GAN) (Fig. 5l, m). To establish whether Fst mediates FoxO1-dependent MASLD/MASH in LDKO mice, we used Albumin-Cre to delete hepatic Irs1, Irs2, and Fst, generating LDKO^{FstKO} mice. Compared to floxed Cntr mice fed the GAN diet for 10 weeks, LDKO^{FstKO} mice had 28% less body mass and 22% less liver mass (Fig. 5n–p). Consistent with the known role of Fst-driven lipolysis to upregulate hepatic glucose production in LDKO mice, glucose tolerance was equivalent in LDKO^{FstKO} and Cntr mice (Fig. 5q)[52]. Serum from LDKO^{FstKO} mice was non-lipemic and serum TAG concentration was normal compared to Cntr mice (Fig. 5r, s). Compatibly, hepatic TAG content and lipid droplets in H&E sections were lower in LDKO^{FstKO} mice, while hepatic FFA was equivalent to Cntr (Fig. 5t–v). Consistent with reduced hepatosteatosis relative to LDKO mice fed the GAN diet, fibrosis was not detected by Masson trichrome staining of LDKO^{FstKO} liver

https://doi.org/10.1038/s41467-025-66296-5

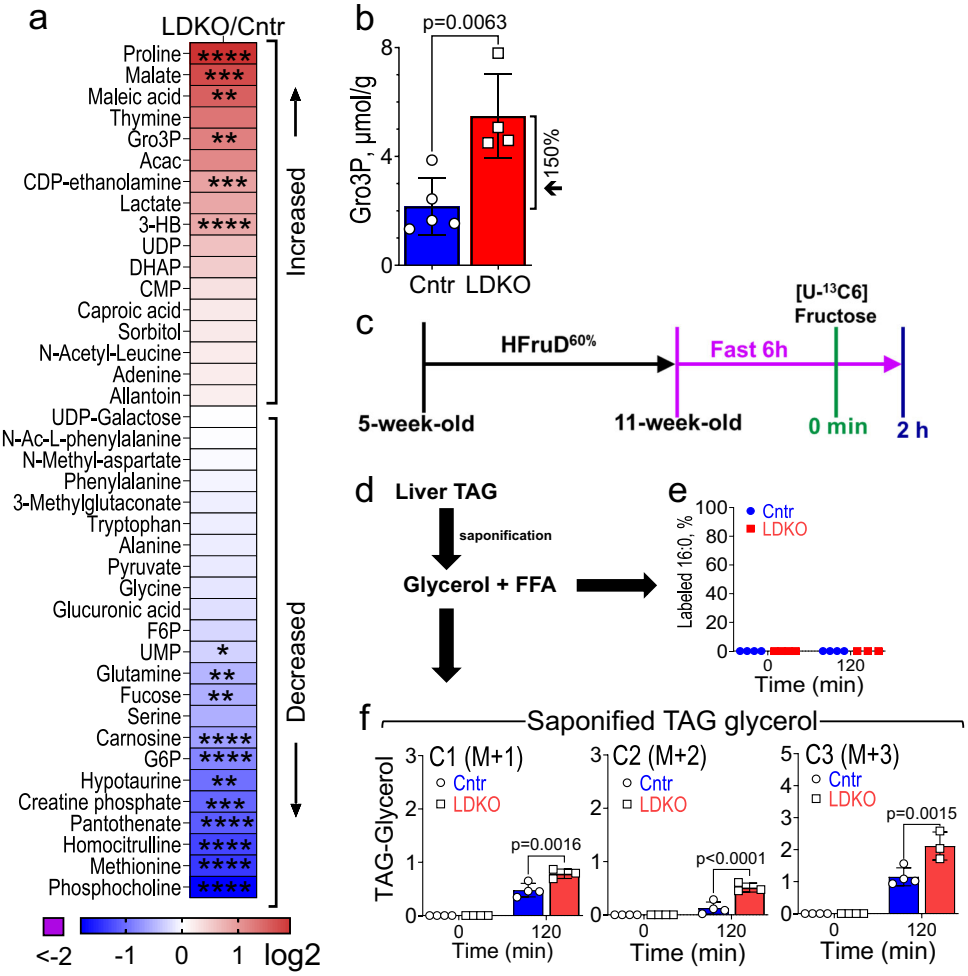

Fig. 4 | Fructose potentiates hepatic re-esterification of FFA in LDKO mice. Mice were weaned onto chow at 3 weeks and placed on the HFruD$^{60\%}$ at 5 weeks. **a** The abundance of polar metabolites was determined by LC-MS from liver extracts of 11-week-old Cntr and LDKO mice fasted for 6 hrs ($n = 4$). **b** Liver Gro3P content was measured by Gro3P assay kit in liver extracts from 11-week-old Cntr or LDKO mice ($n = 5, 4$). **c** Fasted (5 hrs) 11-week-old Cntr and LDKO mice were gavaged once with 2 g/kg of [U-^{13}C6]fructose and 2 hrs later the liver was dissected and extracted into 0.7 ml 40:40:20 acetonitrile:methanol:H_2O and 1 mL hexane for saponification. **d** Organic (FFA) and aqueous (Gro3P) phases were analyzed by LC-MS. **e** Incorporation of [^{13}C] into 16:0 FFA ($n = 3$-4). **f** Incorporation of [^{13}C] into glycerol. C1 (M + 1), C2 (M + 2), and C3 (M + 3) TAG-glycerol (%) were quantified using LC-MS and multiplied by total TAG (mg/g liver) to calculate the labeled TAG-glycerol per gram of extracted liver ($n = 4, 4, 4, 3$). Data are means ± SEM. *P* values were obtained from (**b**) two-tailed unpaired t-test or (**f**) two-way ANOVA. Source data are provided in the Source Data file.

sections (Fig. 5w). Thus, adipose IR and lipolysis promoted by hepatic Fst was required for acute MASLD/MASH in LDKO mice fed the GAN diet.

Gain or loss of hepatic Fst function oppositely modulates MASLD in mice fed HFruD$^{60\%}$

Next, we investigated whether exogenous Fst could promote MASLD in wild-type mice with intact hepatic insulin signaling. Wild-type C57BL6 mice were fed HFruD$^{60\%}$ for 2 months before infection with hepato-specific Fst315$^{AAV\cdot TBG}$ virus (Fst315 mice) or control GFP$^{AAV\cdot TBG}$ virus (GFP mice). After two more months on HFruD$^{60\%}$, circulating Fst increased about 3-fold in Fst315 mice, as previously observed (data not shown)[52]. The Fst315 mice had a 22% larger liver than control GFP mice, with 61% higher TAG mass and more lipid droplets in H&E sections (Supplemental Fig. S8a–d). To further confirm that Fst promotes hepatic steatosis in mice with normal hepatic insulin signaling, we generated LFst^{KO} mice (Fst$^{L/L}$•Cre^{Alb}) lacking only hepatic Fst. The LFst^{KO} mice and floxed Cntr mice (Fst$^{L/L}$) were fed HFruD$^{60\%}$ for 10 weeks. Liver mass trended slightly lower in LFst^{KO} mice (-6%, $p = 0.06$) (Supplemental Fig. S8e, f); however, liver sections from LFst^{KO} mice had fewer lipid droplets and 27% ($p = 0.03$) less TAG than Cntr (Fst$^{L/L}$) mice (Supplemental Fig. S8g, h). Thus, gain or loss of hepatic Fst function oppositely modulated hepatic lipid accumulation during HFruD$^{60\%}$ in mice with intact hepatic insulin signaling.

Hepatic Fst315$^{AAV\cdot TBG}$ accelerates MASLD/MASH in C57BL6 mice fed GAN diet

Liver fibrosis is a key pathologic feature of MASH[67,88]. Previous work shows that mild fibrosis develops in C57BL6 mice fed the GAN diet between 5 to 24 weeks, which progresses to stage 3 fibrosis by 48 weeks[22,89]. To investigate whether exogenous Fst could accelerate fibrotic MASH in mice with intact hepatic insulin signaling, we fed C57BL6 mice GAN diet for 9 months, infecting them after 7 months on diet with Fst315$^{AAV\cdot TBG}$ (Fst mice) or control GFP$^{AAV\cdot TBG}$ (GFP mice). Compared to GFP mice, serum Fst was about 3-fold higher in Fst315 mice, comparable to serum Fst levels in LDKO mice (Fig. 6a)[52]. Seven weeks after infection, fasting glucose increased, and glucose tolerance decreased in Fst315 mice compared to GFP mice (Fig. 6b, c). Two months after infection, mice were sacrificed for analysis. Compared to uninfected Cntr mice fed chow, both GFP and Fst315 mice fed GAN diet had increased liver mass (Fig. 6d). However, compared to GFP mice, the Fst315 mice had a larger liver that contained more TAG, FFA, and

https://doi.org/10.1038/s41467-025-66296-5

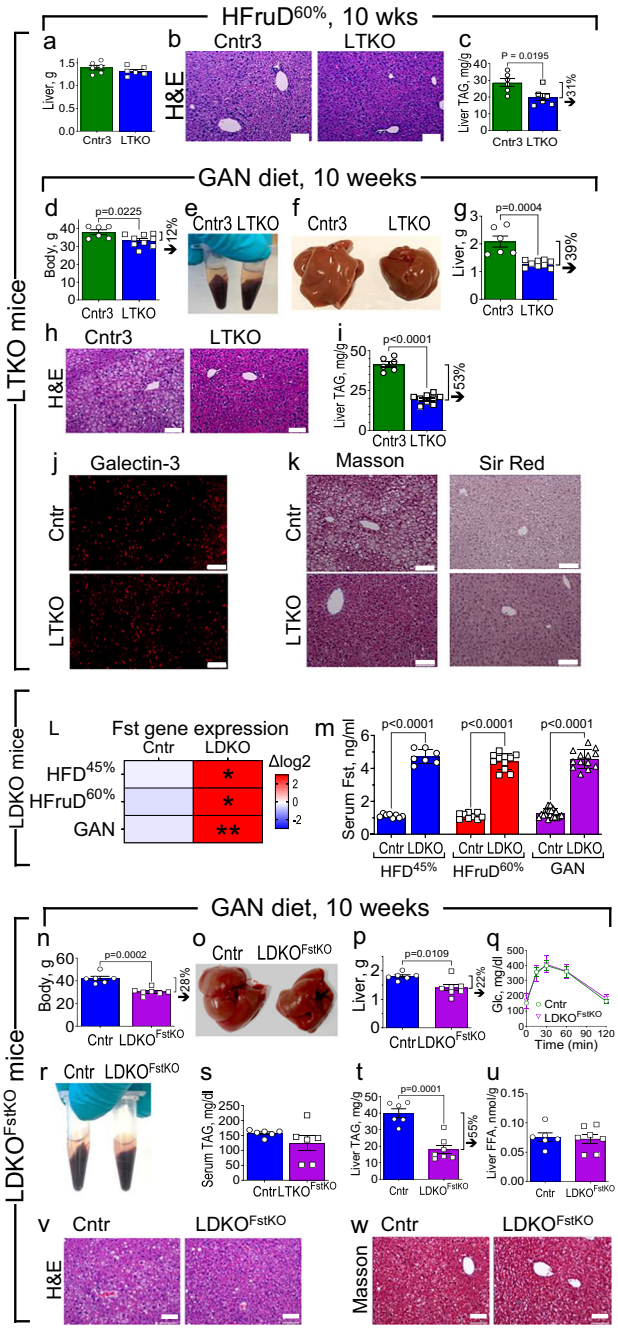

Fig. 5 | Hepatic FoxO1→Fst promotes MASLD/MASH in LDKO mice fed HFruD$^{60\%}$ or GAN diet. Mice were fed HFruD$^{60\%}$, GAN diet, or HFD$^{45\%}$ beginning at age 5 weeks. **a**–**c** Cntr3 (Irs1$^{L/L}$•Irs2$^{L/L}$•FoxO1$^{L/L}$) and LTKO (LDKO•FoxO1$^{L/L}$) mice fed HFruD$^{60\%}$ for 10 weeks: (**a**) liver masses ($n = 6$); **b** representative H&E-stained liver sections ($n = 3$); and (**c**) liver TAG concentrations ($n = 6$). **d**–**k** Cntr3 and LTKO mice fed GAN diet for 10 weeks: **d** body masses ($n = 6,9$); **e** representative photos of centrifuged sera ($n = 3$); (f,g) photos of dissected livers and liver masses ($n = 6, 9$); (**h**) representative H&E-stained liver sections ($n = 4$); **i** liver TAG concentrations ($n = 6, 9$); **j** representative Galectin-3 immunostained liver sections ($n = 4$); **k** representative Masson trichrome or Sirius Red-stained liver sections ($n = 4$). **l**, **m** Liver Fst mRNA ($n = 2$) and corresponding serum Fst concentrations in Cntr and LDKO mice fed HFD$^{45\%}$, HFruD$^{60\%}$, or GAN diet (from left to right: $n = 8, 7, 9, 11, 20, 13$). **n**–**w** Cntr (Irs1$^{L/L}$•Irs2$^{L/L}$•Fst$^{L/L}$) and LDKO^{FstKO} mice (LDKO•Fst$^{L/L}$) fed GAN diet for 10 weeks: **n** body masses ($n = 6, 7$); **o**, **p** representative photos of dissected livers and liver masses ($n = 6, 7$); **q** GTT (1 g/kg glucose, ip) performed after 6 weeks GAN diet ($n = 6, 7$); **r**, **s** representative photos of centrifuged sera ($n = 3$) and serum TAG concentrations ($n = 6$); **t**, **u** liver TAG and FFA concentrations ($n = 6, 7$); **v**, **w** representative H&E and Masson-stained liver sections ($n = 4$). Micrograph scale bars = 100 μm. Data are means ± SEM. *P* values (**a**, **c**–**d**, **g**, **i**, **m**, **n**, **p**, and **s**–**u**) were obtained from two-tailed unpaired t-test. Source data are provided in the Source Data file.

lipid droplets in H&E sections (Fig. 6e–i). Moreover, GAN-promoted fibrosis quantified by Masson or Sirius Red staining was significantly higher in Fst315 mice than in GFP mice (Fig. 6i–k). Unexpectedly, hepatic TC in Fst315 mice was significantly lower than in GFP mice, suggesting that Fst overexpression promoted MASH independent of elevated hepatic cholesterol (Fig. 6h). We conclude that Fst expression similar to that in LDKO mice was sufficient to accelerate MASLD-to-MASH progression in wild-type mice fed the GAN diet.

Circulating FST is associated with impaired adipose insulin sensitivity and higher liver fat in patients

Previously, the TDFS (Tübingen Diabetes Family Study) investigated 210 non-diabetic subjects (88 male, 122 female) with a family history of T2D or other metabolic disease risk factors, revealing a negative correlation of plasma FST with AT-IS (adipose tissue insulin sensitivity) and a positive correlation of FST with liver fat[64]. Because Fst-promoted adipose IR in LDKO mice associates with lower body and adipose mass (see Fig. 1b, c and Supplemental Fig. S3a, b), we split the analysis of serum FST versus AT-IS in TDFS subject groups with a low BMI ($< 25\ kg{\cdot}m^{-2}$) or a high BMI ($\geq 25\ kg{\cdot}m^{-2}$). Compatible with an effect of FST to redistribute TAG from adipose to the liver, the correlation of plasma FST with impaired AT-IS was strongest in the subjects with a low BMI ($n = 32$; $r = -0.38$; $p = 0.02$), but weakest and insignificant in patients with a high BMI ($n = 178$; $r = -0.13$; $p = 0.08$) (Fig. 7a, b). To further investigate the relation of serum FST, AT-IS, and adipose mass with hepatic lipid accumulation, we performed k-means clustering of all 210 subjects, using previously determined serum FST, AT-IS, gluteofemoral adiposity (GF-AT/total AT), and liver fat as variables. Subjects with the highest serum FST (Cluster 1, $n = 79$) had the lowest gluteofemoral fat in conjunction with low AT-IS, and the most liver fat (Fig. 7c–f). Conversely, those with the lowest serum FST (Cluster 3, $n = 58$) had the highest AT-IS and gluteofemoral fat, and the least liver fat (Fig. 7c–f). Given these results, we infer that Fst-dependent adipose lipolysis and acute MASLD/MASH in LDKO mice fed the GAN diet might represent a worst-case intensification of an equivalent mechanism active in some people at risk for T2D and MASLD.

Discussion

IR (insulin resistance) and obesity are usually associated with T2D and MASLD[7]. Regardless, the molecular mechanisms linking IR to MASLD are difficult to understand because complete hepatic IR—modeled in LDKO (Irs1$^{L/L}$•Irs2$^{L/L}$•Cre^{Alb}) or related mice fed chow or a high fat diet—causes diabetes without obesity or liver fat accumulation[25,27,31,33,35,90]. Some investigators have invoked pathway-selective hepatic IR as the root cause of MASLD's close association with IR[27,33,34]; however, as MASLD progresses to MASH and toxic diacylglycerol and ceramide intermediates accumulate[91,92], proximal insulin signaling might approach a state of near-complete IR resembling that in LDKO mice[36]. Importantly, we find that LDKO mice fed the high-fructose GAN diet develop acute diabetes and MASLD/MASH, including severe dyslipidemia, inflammation, and fibrosis with some fatality after 10 weeks on GAN diet[22,65,66]. Thus, compared to a chow or high-fat diet, the GAN diet accelerates the progression of MASLD/MASH during complete hepatic IR. A simpler high-fructose diet (HFruD$^{60\%}$)—lacking high fat and added cholesterol in the GAN diet—also accelerates MASLD in LDKO mice, but without acute transition to acute fibrotic and inflammatory MASH.

Selective IR is a liver-centric theory of hepatic lipid deposition in which sustained insulin-driven DNL is key[30]. Lower absolute rates of glucose-stimulated hepatic DNL recently measured in patients with MASLD might still contribute to MASLD development, given a real-world chronic excess of lipogenic substrates derived from dietary

sugars[36]. However, only around 25% of fatty acids in hepatic TAG from patients with MASLD are estimated to derive from hepatic DNL, versus around 60% from hepatic re-esterification of circulating FFA[48]. High fructose diets increase the risk of MASLD during hepatic IR[22,74,75], and bolus fructose promotes DNL in human liver without increasing insulin[36]. Regardless, since LDKO mice manifested lower hepatic DNL relative to control mice—even as both consumed a high-fructose diet—we infer that hepatic DNL is not the primary cause of accelerated MASLD in LDKO mice fed HFruD$^{60\%}$, or acute MASLD/MASH in LDKO mice fed the GAN diet. Instead, adipose IR and lipolysis caused by hepatic Fst expression and secretion appears to drive MASLD/MASH in LDKO mice fed the GAN diet. Both endogenous hepatic Fst in LDKO mice and exogenous (viral) Fst in wild-type mice were previously shown to stimulate HGP through lipolytic release of FFA from adipose[52]. Our present findings demonstrate that Fst-promoted lipolysis also accelerates MASLD progression, but in a fructose-dependent manner. Considering this dependence, we note that HFruD$^{60\%}$ or GAN did not, in general, restore impaired expression of DNL genes in LDKO mice; nor did it have a differential effect upon expression of fructose metabolic genes (including Chrebp), or enhance expression of genes involved in hepatic FFA uptake or esterification. Thus, we infer that fructose metabolism in LDKO mice is particularly effective at potentiating hepatic TAG formation through re-esterification of circulating FFA. This FFA-driven patho-mechanism is compatible with other data showing that infused FFA can drive hepatic lipid deposition in wild-type mice independent of insulin[49].

The evident means by which fructose potentiates TAG formation in the LDKO liver is by provision of Gro3P to which incident FFA can be esterified. LC-MS analysis of saponified TAG from LDKO mice after gavage with oral [U-^{13}C6]fructose reveals increased labeling of fully and partially labeled Gro3P, whereas [^{13}C]fatty acids in TAG are never detected. Moreover, enzymatic assay of Gro3P in liver lysates reveals higher steady-state Gro3P in liver of LDKO mice fed HFruD$^{60\%}$. Since Gro3P is in redox equilibrium via the glycerol-phosphate shuttle with DHAP (a product of fructolysis by Aldob), Gro3P accumulation might involve a more reducing environment in the liver of LDKO mice[93]. We hypothesize that a key factor giving rise to increased hepatic Gro3P in LDKO mice is the chronically gluconeogenic state of the insulin resistant liver of LDKO mice. This state owes both to FoxO1-dependent upregulation of gluconeogenic gene expression and to strong down-regulation of Gck (glucokinase)[29]. In LDKO mice fed chow or a low-fructose HFD, hepatic production of 3-carbon glycolytic intermediates or equivalent Gro3P might be somewhat diminished owing to minimal Gck activity[29]. By contrast, in LDKO mice fed GAN or HFruD$^{60\%}$, intact fructose or its intestinal metabolites that reach the liver via the portal circulation can increase hepatic DHAP and Gro3P through either Aldob-mediated fructolysis or gluconeogenic formation of DHAP, respectively. In brief, factors differentiating LDKO from control mice fed high-fructose diets include both higher circulating FFA and hepatic Gro3P, resulting in accelerated MASLD in LDKO mice only.

Fructose metabolism depends upon its phosphorylation by high affinity Khk-C, which is found in the liver, intestine and kidney[94]. To differentiate the effects of hepatic and intestinal fructose metabolism on MASLD in LDKO mice, we deleted Khk in LDKO^{KhkKO} mice and found that hepatic fructose phosphorylation was not required for acute MASLD during the GAN diet. Although we did not perform metabolic tracing experiments in LDKO^{KhkKO} mice, this result suggests that sufficient Gro3P to support excess TAG formation was produced in LDKO^{KhkKO} mice through gluconeogenic use of lactate, alanine, and other less abundant fructose metabolites delivered to the liver by intestinal fructose metabolism[94]. Similar MASLD progression in LDKO and LDKO^{KhkKO} mice on GAN diet is not entirely unexpected, as the mouse intestine directly metabolizes most ingested fructose, and also adapts to high-fructose consumption to maximize its absorption and metabolism[94].

Recent studies document similar changes in hepatic transcription in MASH patients and C57BL6 mice fed the GAN diet for 38-42 weeks—including genes involved in inflammatory signaling, endoplasmic reticulum (ER) stress, hepatocellular injury, and ECM remodeling (fibrosis)[66]. Analysis of hepatic RNA expression in LDKO mice fed HFruD$^{60\%}$ diet for just 10 weeks revealed a modest upregulation of MASLD/MASH-associated gene sets, which was strikingly greater in LDKO mice fed GAN diet. The top three liver gene set changes found by unbiased iPathway analysis in LDKO mice fed the GAN diet include 'chemokine signaling', 'miRNA changes associated with regulation of cancer', and 'NF-kB signaling'. Chemokine signals are important regulators of cell trafficking, including hepatic recruitment of circulating monocytes[95]. Consistently, expression of genes having a known association with monocyte recruitment also increased strongly in LDKO mice fed the GAN diet. Chronic inflammation is one of the strongest independent predictors of MASH, fibrosis, cirrhosis, and HCC[96,97]. Genes associated with hepatic NFkB signaling were upregulated in LDKO mice on GAN diet, affecting immunity, inflammation and cell survival; Tlr4 (Toll Like Receptor 4) upregulated in this gene set is known to play a role in fructose-induced MASLD[98]. Other sets of genes involved in signaling by inflammatory cytokines TNFα and IL17 also increased in liver of LDKO mice fed GAN diet. Finally, TNFα is reported to synergize with cholesterol (enriched in the GAN diet) to cause mitochondrial dysfunction and liver damage[97,99].

Inflammation involving factors such as IL17 can drive the activation of HSCs (hepatic stellate cells) that modulate immune mechanisms via chemokines and cytokines, or transdifferentiate into matrix-producing myofibroblasts[96]. Expression of genes associated with ECM organization and fibrosis increases strongly in LDKO mice fed GAN diet, consistent with fibrosis revealed by Sirius Red and Masson staining. Thus, complete hepatic IR in LDKO mice fed GAN diet acutely exacerbates known inflammatory and fibrotic pathways upregulated by the GAN diet and in MASH patients[66,80,100]. Whether deletion of FoxO1 (LTKO mice) or Fst (LDKO^{FstKO} mice) attenuates inflammatory gene expression seen in LDKO mice on GAN diet remains to be investigated; however, either deletion was sufficient to block acute progression to MASH.

Since MASLD and its progression to MASH is strongly associated with obesity, the rapid progression of MASLD in lean LDKO mice seems contrary to expectations[6]; however, hepatic Fst secretion inhibits myostatin in LDKO mice, promoting muscle energy expenditure and an overall lean body phenotype[53,101]. Consistently, a significant subset of lean adult subjects also develops MASLD and its life-threatening sequelae when triglycerides are poorly sequestered by insufficient or insulin-resistant WAT, integrating partial lipodystrophy with hepatic steatosis[41,46,102,103]. Interestingly, a *GCKR* (Glucokinase Regulatory Protein) variant that promotes FST secretion from hepatocytes in vitro associates with plasma FST levels and more than 25 other metabolic traits including T2D and MASLD[64]. Moreover, in patients predisposed to metabolic disease in the TDFS (Tübingen Diabetes Family Study), circulating FST was higher in subjects with MASLD[64]. Our analysis of the TDFS cohort suggests that higher circulating FST is associated with the redistribution of peripheral gluteofemoral fat to the liver. Although this relation is not as strong as in LDKO mice, it suggests a mechanism linking circulating FST with reduced peripheral adipose mass and increased liver fat in subjects with metabolic disease[64]. Thus, future strategies to reduce MASLD incidence and its progression to MASH might include attenuation of hepatic FST secretion to reduce adipose lipolysis and restore healthy liver-adipose crosstalk[51].

A technical limitation of our work herein is that we did not genetically or pharmacologically block adipose lipolysis in LDKO mice to interrupt the proposed mechanism of Fst-promoted lipolysis and hepatic FFA re-esterification as the cause of acute MASLD in fructose-fed LDKO mice. However, we previously demonstrated that Fst promotes adipose insulin resistance and lipolysis in chow-fed LDKO

https://doi.org/10.1038/s41467-025-66296-5

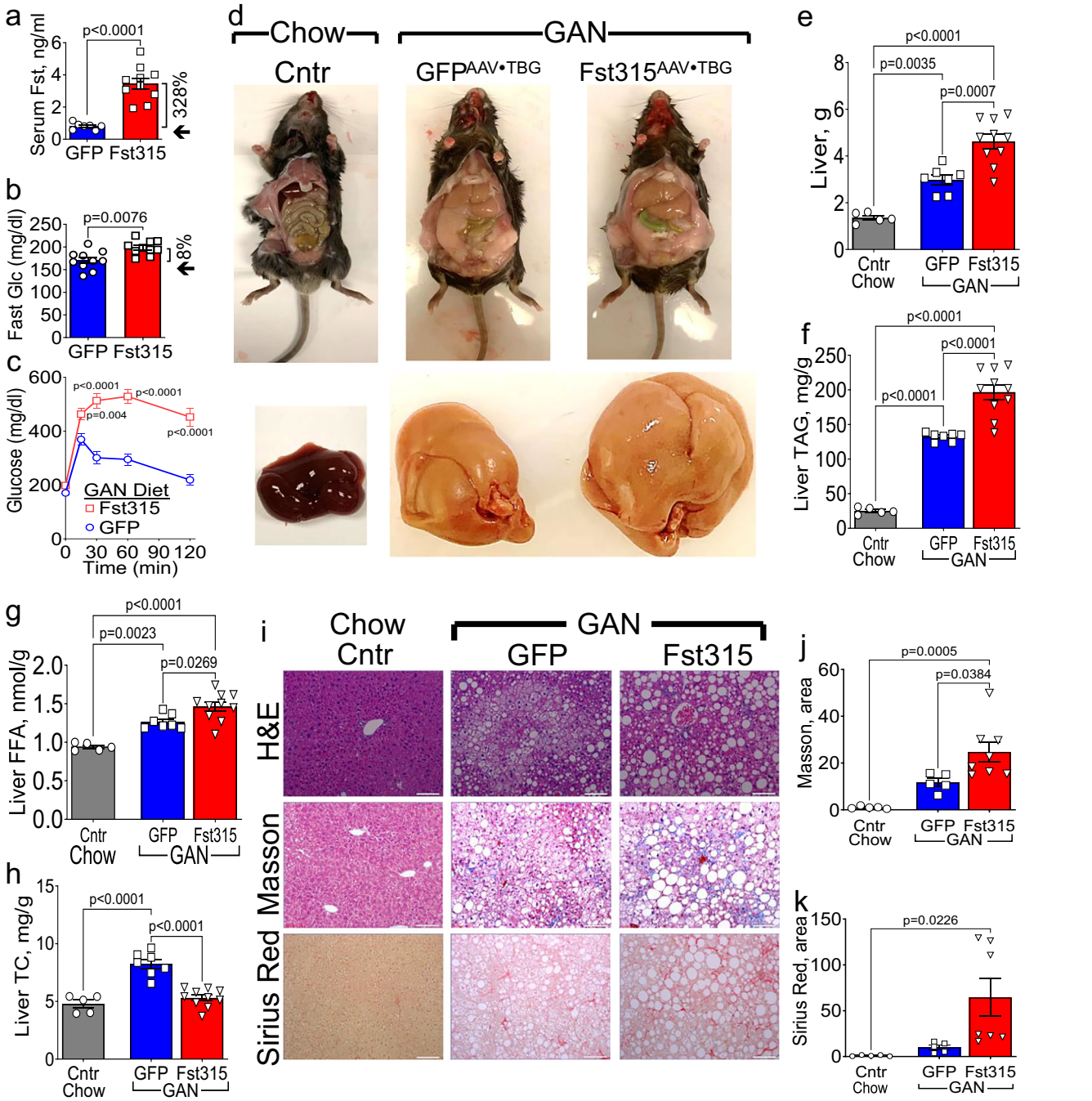

Fig. 6 | Hepatic Fst promotes MASLD/MASH in C57BL/6 mice fed GAN diet. Mice were weaned onto chow at 3 weeks, placed on GAN diet at 5 weeks, and infected without or with GFP$^{AAV•TBG}$ (GFP mice) or Fst315$^{AAV•TBG}$ (Fst315 mice) after 7 months on GAN diet. **a** Serum Fst levels determined in 9-month-old GFP mice ($n = 7$) and Fst315 mice ($n = 10$). **b**, **c** Fasting (6-hr) blood glucose and GTT (1 g/kg glucose, ip) performed on GFP or Fst315 mice 7 weeks after infection ($n = 10$). **d** Representative photographs of dissected 9-month-old mice and their livers, including Cntr mice fed chow and GFP or Fst315 mice fed GAN diet. **e**–**h** Liver masses and hepatic TAG, FFA, and TC concentrations determined in 9-month-old Cntr mice fed chow, or GFP and Fst315 mice fed GAN diet ($n = 5, 7, 10$). **i** Representative liver sections from 9-month-old mice stained by H&E, Masson, or Siris Red ($n = 4$, scale bar= 100 μm). (**j**,**k**) Masson and Sirius Red staining of liver sections quantified by Image J ($n = 5, 5, 7$). Data are means ± SEM. *P* values were obtained from (**a**, **b**) two-tailed unpaired t-test, (**c**) two-way ANOVA, or (**e**–**h**, **j**–**k**) one-way ANOVA. Source data are provided in the Source Data file.

mice[52], and show herein that acute MASLD in LDKO mice fed HFruD$^{60\%}$ or GAN is eliminated by hepatic disruption of either Fst or its upstream IRS-regulated transcriptional activator FoxO1. Another technical limitation is that GAN and HFruD$^{60\%}$ diets do not directly model a typical human diet and are instead designed to accentuate a physiologic response or elicit MASLD/MASH on a manageable time scale. An important distinction limiting direct translation of our results to MASLD in humans is that LDKO mice exhibit 'complete hepatic insulin resistance', in which the persistent or elevated insulin-driven hepatic lipogenesis that characterizes 'selective insulin resistance' in humans is absent. Related to this point, we infer (above) that increased hepatic Gro3P and FFA re-esterification in fructose-fed LDKO mice depend upon a chronic gluconeogenic state of hepatic gene expression and glucose metabolism. This state is unlikely to be as complete or

https://doi.org/10.1038/s41467-025-66296-5

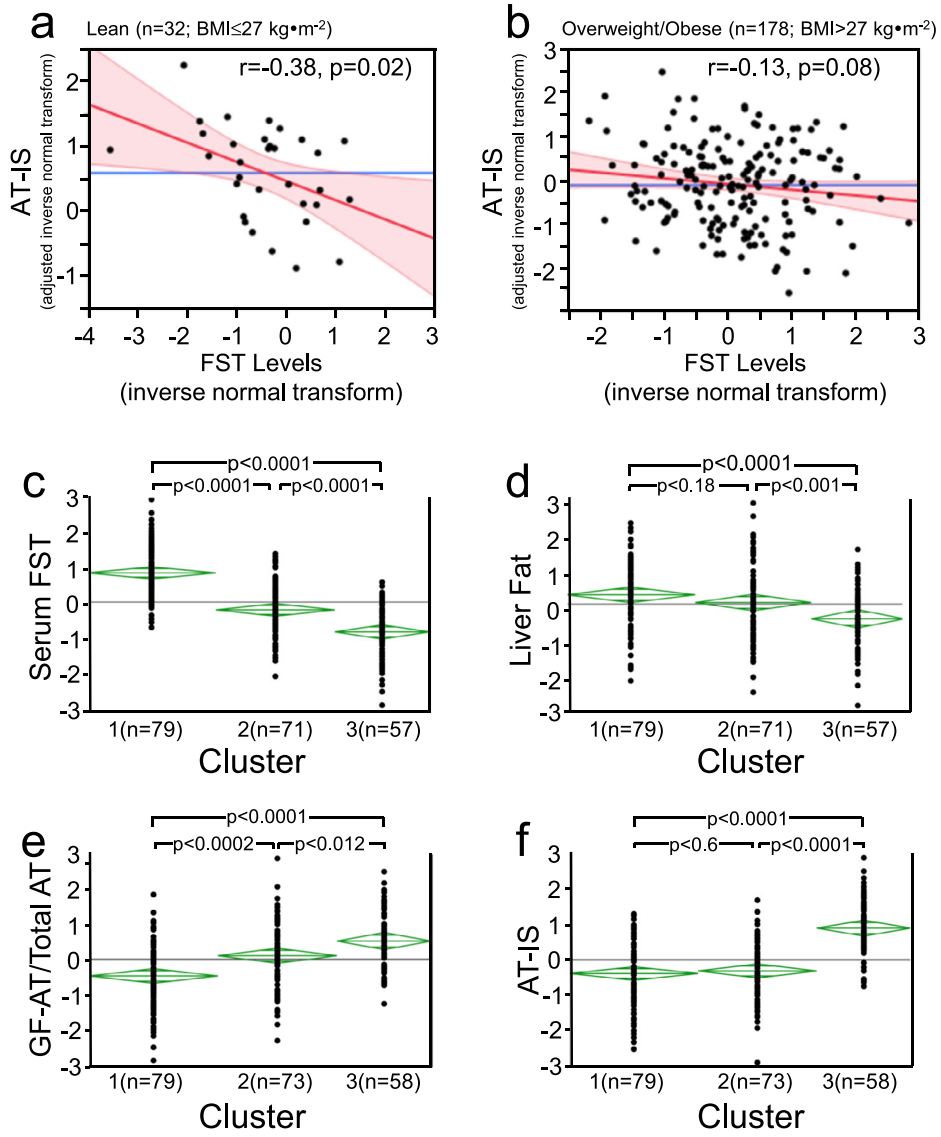

Fig. 7 | Association of circulating FST with AT-IS (adipose insulin sensitivity), fat distribution, and liver fat in humans. (**a**,**b**) Multivariate linear regression of inverse normalized AT-IS (adjusted for age, sex, and body fat mass) against circulating inverse normalized FST for individuals without obesity (BMI < 25 kg·m^{-2}) and individuals with overweight or obesity (BMI ≥ 25 kg•m^{-2}). (**c**-**f**) k-means clustering to establish the relation between gluteofemoral fat, liver fat, AT-IS and circulating FST using cubic clustering criterion (JMP 16.2.0, SAS) to identify 3 clusters[76]. Data are means ± SEM.

persistent in many humans with MASLD, unless effectively promoted by genetic predisposition to adipose insulin resistance and lipolysis. Thus, further studies that directly assess the role of FST upon MASLD progression in lean subjects might be particularly useful.

Methods

Mice

All mouse experiments reported in this study received approval from the Boston Children's Hospital Institutional Animal Care and Use Committee (IACUC Approval # 00002602; PHS Animal Welfare Assurance Number: A3303-01). All mice were maintained on a 12 h light/12 h dark cycle (lights on at 7:00 a.m.) at an ambient temperature of 22 °C and 60% relative humidity. The mouse environment was enriched by a shredded paper nestlet that the mice turn into a nest. Single housing was tracked carefully, and these cages have a 'mouse house', which is a light-blocking polycarbonate dome they can get under. We performed animal experiments according to procedures approved by the Boston Children's Hospital Institutional Animal Care and Use Committee. We generated liver specific Irs1 and Irs2 double knockout (LDKO), and Irs1, Irs2 and FoxO1 triple knockout (LTKO) mice as previously described[29,93]. We purchased C57BL6/J mice (Stock No. 000664) and B6;FVB-Tg(Adipoq-cre)1Evdr/J mice (Stock No. 010803) from The Jackson Lab. B6;FVB-Tg(Adipoq-cre)1Evdr/J was from Jackson lab, stock no. 010803. We generated FDKO mice by cross breeding B6;FVB-Tg(Adipoq-cre)1Evdr/J with Irs1 and Irs2 double floxed mice. Fst$^{L/L}$ mice were from Dr. Matzuk, Baylor College of Medicine. We generated Fst-LKO and LDKO^{FstKO} by cross breeding Fst$^{L/L}$ with Cre^{Alb} or LDKO mice. Khk$^{L/L}$ mice were from Dr. Miguel Lanaspa, University of Colorado. We generated Khk-LKO and LDKO^{KhkKO} by cross breeding Khk$^{L/L}$ with Cre^{Alb} or LDKO mice. qPCR primers for KHK mice genotyping are described[87].

Diets

Before initiation of diet studies, the mice were maintained on a standard laboratory chow diet (Prolab Isopro RMH 3000, LabDiet, St. Louis, Catalog #5P75) containing 7 kcal% from simple sugars, 3 kcal% from fat, 50 kcal% from polysaccharide, and 15 kcal% from protein. High-fat diet (Research Diet: R1245i) contains 45 kcal% from fat, 20 kcal % from protein, 35 kcal% carbohydrate. High-fructose diet (Harlan Teklad: TD.89247) contains 13 kcal% from fat, 20 kcal% from protein,

66 kcal% from carbohydrate (including 60% fructose). GAN diet (Research Diet: D09100310) contains 40 kcal% from fat, 20 kcal% from protein, 20 kcal% from fructose; 10 kcal% from sucrose; and 2% cholesterol.

Glucose tolerance tests (GTT)

For GTTs, mice were fasted, but with free access to water, for 5 h before the procedure. At the start of the procedure, the mice were weighed, and basal glucose levels were taken. The mice were then injected intraperitoneally with glucose (1 or 2 g/kg body weight) 6 h after fasting. Glucose levels were measured again at times 15, 30, 60 and 120 min after injection.

Histological and immunohistochemical analyses

Liver and WAT were fixed in phosphate buffered paraformaldehyde (10%) and embedded in paraffin or OCT. H&E staining, Masson staining, Sir red, and Oil Red staining were conducted by the Pathology Core at Dana-Farber Harvard Cancer Center. Composite images were created from a 10 × 10 array of adjacent non-overlapping ×10 magnification images with an Axiovert Zeiss LSM 510 microscope.

Blood chemistry analysis

We used commercial ELISA kits to measure circulating insulin level according to the manufacturers' instructions. Insulin kit (80-INSMSU-E01) was purchased from Alpco Inc. Liver Gro3p concentration was measured by Elisa assay kit (ab174094) from Abcam. Cholesterol. free fatty acids, and triglycerides were measured using commercial assay kits (Wako USA). Blood glucose was measured using a glucose meter (Contour from Bayer).

Tissue lipid extraction

Around 75 mg of liver tissue was homogenized in 1 mL 50 mM NaCl on ice, following the addition of 5 mL of chloroform/methanol mixture (chloroform: methanol = 2:1). The homogenized tissue solution was centrifuged at 1000 × g for 10 min before vortexed for 30 s. The aqueous phase was carefully removed, and the left oleic phase was mixed with 1.5 mL of methanol. The resulting mixture was vortexed for 30 s and centrifuged at 1,000 × g for 10 min. The lipid extract (500 µl) was carefully moved to a new tube and dried in fume hood. The resulting pellet was dissolved 10% Triton X-100 in acetone and used for TG, TC, and FFA determination with assay kit according to manufacture instructions.

De novo lipogenesis

De novo lipogenesis in mouse liver was measured essentially as described previously[104]. Briefly, mice are fasted for 16 h overnight. Next morning, the animals are fed on a diet for 4 h. 3H2O (15 uCi/g, diluted in 200 ul saline) is injected intraperitoneally. One hour later, mice are sacrificed after they are anaesthetized with ketamine/xylazine. Blood samples and liver lipids were extracted for isotope analysis.

AAV virus vector preparation

AAV8.TBG.PI.eGFP (GFPAAV•TBG, Lot: AV-8-PV0146) were purchased from the Vector Core, University of Pennsylvania. To make overexpression AAV viruses, mouse gene Fst315 coding sequences were cloned into a pAAV2 backbone with TBG promoter vector and then sent to BCH viral core for AAV2/8 virus production and purification[52].

AAV Viruses injection to mice

A virus was introduced to mice through the tail vein injection. The virus was thawed at 25 °C before injection and the desired amount of virus was diluted with PBS to a final volume of 100 µL per mouse. To prevent the back flow of virus solution, mild pressure was applied at the spot of injection immediately after injection until no bleeding was achieved.

Primary hepatocytes

Two-month-old male mice were anesthetized by intraperitoneal injection of ketamine/xylazine (100 mg/kg and 10 mg/kg body weight). Following anesthesia, the abdominal cavity was opened by scissors and the vena cava and portal vein were located. A perfusion catheter was placed in the vena cava. Pre-warmed Liver Perfusion Medium (Invitrogen, 17701) (37 °C) was delivered at 2.5 ml/min for 5 min using a peristaltic pump. An incision was made at the portal vein as an outlet for the perfusion solution. Immediately following the Liver Perfusion Medium, pre-warmed Liver Digest Medium (Invitrogen, 17703) (37 °C) was delivered at 2.5 ml/min for 5 min using a peristaltic pump. At the end of the perfusion, the liver was dissected and transferred to a Petri dish on ice containing 10 ml of L-15 medium (Invitrogen, 21083) with 10%FBS. After washing three times with Hepatocyte Wash Buffer (Invitrogen, 17704), the primary hepatocytes were re-suspended in William's E medium (Invitrogen, 12551) containing Percoll (Sigma, p4937). After plating on collagen I-coated plates for 4 hrs in William's E medium containing 10%FBS/PenStrep at 37 °C, the unattached cells were removed, and the dishes were washed with PBS and incubated with William's E medium containing 10%FBS/PenStrep.

DNL in primary hepatocytes

Primary hepatocytes were seeded in a 12-well plate. Prior to isotope labeling, edium was changed to fresh DMEM/high glucose and insulin was added to a final concentration of 100 nM and dexamethasone to a final concentration of 100 nM. 2 ul of [1, 2-14 C]-sodium acetate (0.2 uCi) was added into the culture medium and incubated for 2 h. After washing with PBS, hepatocytes were lysed with 1 N NaOH solution. The lipids were extracted with petroleum ether. Radioactivity in the lipid fraction was counted with a liquid scintillation counter. Lipogenic activity was presented as normalized radioactivity to protein amount.

Western blot analysis

Tissue or cells were homogenized in the lysis buffer (50 mm Hepes, pH 7.5, 150 mm NaCl, 10% glycerol, 1% Triton X-100, 1.5 mm $MgCl_2$, 1 mm EGTA, 10 mm sodium pyrophosphate, 100 mm sodium fluoride, and freshly added protease inhibitor cocktail and phosphatase inhibitor cocktail). Protein extracts were resolved on an SDS-PAGE gel and transferred to nitrocellulose membrane (Bio-Rad). Detection of proteins was carried out by incubations with HRP-conjugated secondary antibodies followed by ECL detection reagents.

In vivo isotope tracing, sample preparation, and metabolite extraction

To quantify fructose metabolism in vivo, LDKO and control mice maintained on $Fru^{60\%}$ for 6 weeks were utilized. After a 6-hour fast (8am-2pm), the mice were gavaged with [U-^{13}C]fructose. Following different time intervals post-gavage, the mice were anesthetized with 3% isoflurane via a nose cone for 1–2 min. Blood samples were then collected and kept on ice, while liver tissues were quickly excised and frozen in liquid nitrogen. Fructose metabolites in circulation and liver tissues were extracted using cold 80% methanol. The extraction process involved incubating the samples at 4 °C for 30 min, followed by vortex and immediate centrifugation at 16,000 g for 10 min at 4 °C. The resulting supernatant was collected and concentrated to dryness using a SpeedVac. The dried pellets were subsequently dissolved in HPLC-grade water for LC-MS analysis.

Tissue metabolite extraction and measurement

Frozen tissue was ground by a Cyromill at cryogenic temperature. Ground tissue (20 mg) was then weighed and mixed with 1 ml −20 °C 80:20 methanol:water (HPLC grade). Extract was then vortexed and centrifuged twice at 16,000 × *g* for 20 min at 4 °C. The supernatant was transferred to a new tube, air-dried in a Speed-Vac and stored at -80 °C until LC-MS analysis.

Metabolomics analysis was performed using a Vanquish U-HPLC system coupled to a Q-Exactive HF-X mass spectrometer (Thermo Fisher) operated in negative ion mode with HESI. Metabolites were separated on a hydrophilic interaction liquid chromatography (iHILIC1-(P) Classic) column using a water–acetonitrile gradient with ammonium carbonate/ hydroxide buffer. MS data were acquired in full-scan mode (70–1000 m/z, 60,000 resolution) and processed in TraceFinder v4.1 using exact mass (5 ppm tolerance) and retention time, matched to an in-house chemical standard library.

The relative abundance ($\sum_{i=0}^{n} i*mi$) of detected polar isotopologue in liver extracts was determined by LC-MS/MS, where n is the number of C atoms in the metabolite; i is the isotopologue; and m is the abundance of the isotopologue i. The FC (Fractional Contribution) of [13 C]Fructose incorporated by liver extracts during 30 and 60 minutes was calculated as $FC = \frac{\sum_{i=0}^{n} i*mi}{n*\sum_{i=0}^{n} mi}$ for each selected glycolytic/TCA cycle intermediate.

Triglycerides determinations by LC-MS

Liver (20 μg) lipids were extracted with 1000 μl of isopropyl alcohol:-chloroform (8:2) and subsequently centrifuged. Lipids were separated on an Agilent 1200 HPLC system using a Waters Acquity UPLC® BEH C18 column with a 45-min gradient of acetonitrile/water/methanol (A) and isopropanol/methanol (B), both containing 0.1% formic acid and 0.028% ammonium hydroxide. The flow rate was 0.2 mL/min, with a column temperature of 45 °C, autosampler at 4 °C, and injection volume of 5 μL. Lipid detection was performed on an Agilent TOF mass spectrometer, and identification was based on accurate mass, retention time, and external standards when available. Triglycerides were quantified relative to the internal standard 2D93-tripalmitin, with calibration curves generated from spiked tripalmitin in pooled plasma to cover endogenous TG levels.

TAG-glycerol backbone measurement

Cryomill-ground mouse liver powder (20-40 mg) was transferred to an Eppendorf tube chilled with dry ice, and extracted into 0.7 mL 40:40:20 ACN:MeOH:H2O, and 1 mL hexane (both at room temperature). The mixture was centrifuged at 16,000 g for 5 min after bead-shake with Cryomill under room temperature for 30 s. The hexane supernatant (700 μL) was transfered to a new 2 mL tube, and centrifuged in a SpeedVac at 45 C for 30 min, producing the TAG hexane extract ready for saponification.

To saponify the lipids, 1 mL 50 mM KOH in methanol was added to the dried hexane TAG extract, mixed by vortex, and incubated at 60 oC for 1 h. After vortex, 65 μL 3 M HCl in methanol was added to the incubated tube and subjected to SpeedVac (60 oC for 2 hrs) to evaporate methanol and aqueous HCL. Water (100 μL) was added to the dried sample and vigorously mixed by vortex, bringing the compounds into solution.

Following TAG extraction and saponification of liver samples, glycerol was enzymatically derivatized into glycerol-3-phosphate before LC-MS analysis. To the saponified sample, 200 μL freshly made enzyme solution containing 2 U/mL glycerol kinase, 25 mM Tris-HCl (pH 8.0), 50 mM sodium chloride, 10 mM magnesium chloride, and 1.5 mM ATP, and incubated at room temperature for 60 min. The reaction was stopped by the addition of 500 μL methanol. The sample was vortexed, and centrifuged at 16,000 g for 10 min. The supernatant was transferred to the HPLC vial, from which 5 μL was injected to the LC-MS.

Chromatographic separation was achieved using Vanquish UHPLC (Thermo Scientific, Waltham, MA, USA) and XBridge BEH Amide XP column (2.5 μm, 2.1 mm × 150 mm) with guard column (2.5 μm, 2.1 mm × 5 mm) (Waters, Milford, MA). The mobile phase A was water: acetonitrile 95:5, and mobile phase B was water: acetonitrile 20:80, with both phases containing 10 mM ammonium acetate and 10 mM ammonium hydroxide. The elution linear gradient was: 0 ~3 min, 100% B; 3.2 ~6.2 min, 90% B; 6.5 ~10.5 min, 80% B; 10.7 ~13.5 min, 70% B; 13.7 ~16 min, 45% B; and 16.5 ~22 min, 100% B, with flow rate of 0.3 mL/min. The autosampler was at 4 °C. The injection volume was 5 μL. Needle wash was applied between samples using methanol: acetonitrile: water at 40: 40: 20. The mass spectrometry used was the Orbitrap Exploris 480 (Thermo Fisher Scientific, San Jose, CA), and scanned from 70 to 1000 m/z with switching polarity. The resolution was 120,000. Glycerol-3-phosphate labeling was analyzed by EI-MAVEN.

TDFS Cohort

TDFS (Tübingen Diabetes Family Study) is an observational study of 210 Caucasians from the southern part of Germany. Informed written consent was obtained from all participants and the Ethics Committee at the Medical Faculty of the Eberhard Karls University and at the University Hospital of Tübingen approved the protocol. All individuals underwent a 75-g oral glucose tolerance test (OGTT). The adipose tissue insulin sensitivity index proposed by Belfiore et al. was calculated (2/[(InsAUC (0, 60, 120).FFAAUC (0, 60, 120)) + 1]). Total body, visceral and subcutaneous fat mass were measured by magnetic resonance (MR) tomography, with an axial T1-weighted fast spin echo technique with a 1.5 T whole body imager (Magnetom Sonata, Siemens Medical Solutions). Subcutaneous abdominal fat mass and leg fat mass were presented as percentage of total fat mass. Liver fat content was measured by localized 1H-MR spectroscopy. Nonalcoholic fatty liver disease (NAFLD) was defined as a liver fat content >5.56%. Circulating follistatin was measured by a human Follistatin ELISA kit (DFN00, R&D Systems).

Statistical analysis

Two-tailed unpaired Student t tests were used to assess statistical significance between two groups. Multiple groups or treatment were compared using one-way ANOVA or two-way ANOVA. Kruskal-Wallis test was used to assess statistical significance. When ANOVA indicated a significant difference among the groups, the statistical difference between the two groups was compared using a stricter criterion for statistical significance according to the Bonferroni rule. For all test of significance, n indicates individual biological replicates.

Reporting summary

Further information on research design is available in the Nature Portfolio Reporting Summary linked to this article.

Data availability

All in vitro and animal data supporting the findings of this study are available within this article, and its supplementary material. Source data are provided in the Source data file or relevant data repositories. The RNA-seq data from mouse samples produced in this paper have been deposited in the GEO database under accession number GSE270246. Uncropped western blots, analyzed metabolites and their corresponding data, and the values that were used to create all graphs in this paper can be found in the accompanying “Source data” file. For the Tübingen Diabetes Family Study (TDFS), German legislation imposes restrictions on public availability of datasets containing pseudonymized information for the TDFS cohort. The full datasets can be accessed from Dr. Norbert Stefan, University of Tübingen (Norbert.Stefan@med.uni-tuebingen.de). Data access will be granted upon completion of a formal data use agreement review by Dr. Norbert Stefan and the TDFS steering committee. Source data are provided with this paper.

References

1. Rinella, M. E. et al. A multisociety Delphi consensus statement on new fatty liver disease nomenclature. *Hepatology* **78**, 1966–1986 (2023).

2. Brumbaugh, D. E. et al. Intrahepatic fat is increased in the neonatal offspring of obese women with gestational diabetes. *J. Pediatr.* **162**, 930–936 e931 (2013).
3. Wong, R. J. et al. Nonalcoholic steatohepatitis is the second leading etiology of liver disease among adults awaiting liver transplantation in the United States. *Gastroenterology* **148**, 547–555 (2015).
4. Mosca, A. et al. Beverage consumption and paediatric NAFLD. *Eat. weight Disord.: EWD* **21**, 581–588 (2016).
5. Younossi, Z. et al. Global burden of NAFLD and NASH: trends, predictions, risk factors and prevention. *Nat. Rev. Gastroenterol. Hepatol.* **15**, 11–20 (2018).
6. Sheka, A. C. et al. Nonalcoholic steatohepatitis: a review. *Jama* **323**, 1175–1183 (2020).
7. Loomba, R., Friedman, S. L. & Shulman, G. I. Mechanisms and disease consequences of nonalcoholic fatty liver disease. *Cell* **184**, 2537–2564 (2021).
8. Petersen, M. C. & Shulman, G. I. Mechanisms of insulin action and insulin resistance. *Physiol. Rev.* **98**, 2133–2223 (2018).
9. Chaurasia, B. et al. Targeting a ceramide double bond improves insulin resistance and hepatic steatosis. *Science* **365**, 386–392 (2019).
10. Azzu, V., Vacca, M., Virtue, S., Allison, M. & Vidal-Puig, A. Adipose tissue-liver cross talk in the control of whole-body metabolism: implications in nonalcoholic fatty liver disease. *Gastroenterology* **158**, 1899–1912 (2020).
11. Younossi, Z. M. & Henry, L. Epidemiology of non-alcoholic fatty liver disease and hepatocellular carcinoma. *JHEP Rep.* **3**, 100305 (2021).
12. Hosokawa, Y. et al. Adipose tissue insulin resistance exacerbates liver inflammation and fibrosis in a diet-induced NASH model. *Hepatol Commun.* **7**, e0161 (2023).
13. Lotta, L. A. et al. Integrative genomic analysis implicates limited peripheral adipose storage capacity in the pathogenesis of human insulin resistance. *Nat. Genet.* **49**, 17–26 (2017).
14. Eslam, M., Valenti, L. & Romeo, S. Genetics and epigenetics of NAFLD and NASH: Clinical impact. *J. Hepatol.* **68**, 268–279 (2018).
15. Eslam, M. & George, J. Genetic contributions to NAFLD: leveraging shared genetics to uncover systems biology. *Nat. Rev. Gastroenterol Hepatol* **7**, e0161(2019).
16. Romeo, S., Sanyal, A. & Valenti, L. Leveraging human genetics to identify potential new treatments for fatty liver disease. *Cell Metab.* **31**, 35–45 (2020).
17. Younossi, Z. M. et al. Global epidemiology of nonalcoholic fatty liver disease-Meta-analytic assessment of prevalence, incidence, and outcomes. *Hepatology* **64**, 73–84 (2016).
18. Czech, M. P. Insulin action and resistance in obesity and type 2 diabetes. *Nat. Med.* **23**, 804–814 (2017).
19. Jensen, T. et al. Fructose and sugar: a major mediator of non-alcoholic fatty liver disease. *J. Hepatol.* **68**, 1063–1075 (2018).
20. Younossi, Z. M. et al. The global epidemiology of NAFLD and NASH in patients with type 2 diabetes: A systematic review and meta-analysis. *J. Hepatol.* **71**, 793–801 (2019).
21. Softic, S. et al. Fructose and hepatic insulin resistance. *Crit. Rev. Clin. Lab Sci.* **57**, 308–322 (2020).
22. Gallage, S. et al. A researcher's guide to preclinical mouse NASH models. *Nat. Metab.* **4**, 1632–1649 (2022).
23. Trauner, M. & Fuchs, C. D. Novel therapeutic targets for cholestatic and fatty liver disease. *Gut.* **71**, 194–209 (2022).
24. Stefan, N. & Cusi, K. A global view of the interplay between non-alcoholic fatty liver disease and diabetes. *Lancet Diab. Endocrinol.* **10**, 284–296 (2022).
25. Bo, T. et al. Hepatic selective insulin resistance at the intersection of insulin signaling and metabolic dysfunction-associated steatotic liver disease. *Cell Metab.* **36**, 947–968 (2024).
26. White, M. F. & Kahn, C. R. Insulin action at a molecular level - 100 years of progress. *Mol. Metab.* **20**, 101304 (2021).
27. Brown, M. S. & Goldstein, J. L. Selective versus total insulin resistance: a pathogenic paradox. *Cell Metab.* **7**, 95–96 (2008).
28. Biddinger, S. B. et al. Hepatic insulin resistance is sufficient to produce dyslipidemia and susceptibility to atherosclerosis. *Cell Metab.* **7**, 125–134 (2008).
29. Dong, X. C. et al. Inactivation of hepatic Foxo1 by insulin signaling is required for adaptive nutrient homeostasis and endocrine growth regulation. *Cell Metab.* **8**, 65–76 (2008).
30. Cook, J. R., Hawkins, M. A. & Pajvani, U. B. Liver insulinization as a driver of triglyceride dysmetabolism. *Nat. Metab.* **5**, 1101–1110 (2023).
31. Li, S., Brown, M. S. & Goldstein, J. L. Bifurcation of insulin signaling pathway in rat liver: mTORC1 required for stimulation of lipogenesis, but not inhibition of gluconeogenesis. *Proc. Natl. Acad. Sci. USA* **107**, 3441–3446 (2010).
32. Taniguchi, C. M. et al. Divergent regulation of hepatic glucose and lipid metabolism by phosphoinositide 3-kinase via Akt and PKClambda/zeta. *Cell Metab.* **3**, 343–353 (2006).
33. Kubota, N. et al. Differential hepatic distribution of insulin receptor substrates causes selective insulin resistance in diabetes and obesity. *Nat. Commun.* **7**, 12977 (2016).
34. Honma, M. et al. Selective insulin resistance with differential expressions of IRS-1 and IRS-2 in human NAFLD livers. *Int J. Obes. (Lond.)* **42**, 1544–1555 (2018).
35. Shimomura, I. et al. Decreased IRS-2 and increased SREBP-1c lead to mixed insulin resistance and sensitivity in livers of lipodystrophic and ob/ob mice. *Mol. Cell* **6**, 77–86 (2000).
36. Ter Horst, K. W. et al. Hepatic insulin resistance is not pathway selective in humans with nonalcoholic fatty liver disease. *Diab. care* **44**, 489–498 (2021).
37. Sanders, F. W. & Griffin, J. L. De novo lipogenesis in the liver in health and disease: more than just a shunting yard for glucose. *Biol. Rev. Camb. Philos. Soc.* **91**, 452–468 (2016).
38. Chen, Z. et al. Functional screening of candidate causal genes for insulin resistance in human preadipocytes and adipocytes. *Circ. Res* **126**, 330–346 (2020).
39. Younossi, Z. M. et al. Nonalcoholic fatty liver disease in lean individuals in the United States. *Medicine* **91**, 319–327 (2012).
40. Younossi, Z. M., Otgonsuren, M., Venkatesan, C. & Mishra, A. In patients with non-alcoholic fatty liver disease, metabolically abnormal individuals are at a higher risk for mortality while metabolically normal individuals are not. *Metabolism* **62**, 352–360 (2013).
41. Stefan, N., Schick, F. & Haring, H. U. Causes, characteristics, and consequences of metabolically unhealthy normal weight in humans. *Cell Metab.* **26**, 292–300 (2017).
42. Kumar, R. & Mohan, S. Non-alcoholic fatty liver disease in lean subjects: characteristics and implications. *J. Clin. Transl. Hepatol.* **5**, 216–223 (2017).
43. Niriella, M. A. et al. Lean non-alcoholic fatty liver disease (lean NAFLD): characteristics, metabolic outcomes and risk factors from a 7-year prospective, community cohort study from Sri Lanka. *Hepatol. Int.* **13**, 314–322 (2019).
44. Younes, R. & Bugianesi, E. NASH in lean individuals. *Semin Liver Dis.* **39**, 86–95 (2019).
45. Zou, B. et al. Prevalence, characteristics and mortality outcomes of obese, nonobese and lean NAFLD in the United States, 1999-2016. *J. Intern. Med.* **288**, 139–151 (2020).

46. Maier, S. et al. Lean NAFLD: an underrecognized and challenging disorder in medicine. *Rev. Endocr. Metab. Disord.* **22**, 351–366 (2021).
47. Gastaldelli, A., Gaggini, M. & DeFronzo, R. A. Role of adipose tissue insulin resistance in the natural history of type 2 diabetes: results from the san antonio metabolism study. *Diabetes* **66**, 815–822 (2017).
48. Donnelly, K. L. et al. Sources of fatty acids stored in liver and secreted via lipoproteins in patients with nonalcoholic fatty liver disease. *J. Clin. Investig.* **115**, 1343–1351 (2005).
49. Vatner, D. F. et al. Insulin-independent regulation of hepatic triglyceride synthesis by fatty acids. *Proc. Natl. Acad. Sci. USA* **112**, 1143–1148 (2015).
50. Lee, E., Korf, H. & Vidal-Puig, A. An adipocentric perspective on the development and progression of non-alcoholic fatty liver disease. *J. Hepatol.* **78**, 1048–1062 (2023).
51. Stefan, N., Schick, F., Birkenfeld, A. L., Haring, H. U. & White, M. F. The role of hepatokines in NAFLD. *Cell Metab.* **35**, 236–252 (2023).
52. Tao, R. et al. Inactivating hepatic follistatin alleviates hyperglycemia. *Nat. Med.* **24**, 1058–1069 (2018).
53. Tao, R. et al. Hepatic follistatin increases basal metabolic rate and attenuates diet-induced obesity during hepatic insulin resistance. *Mol. Metab.* **71**, 101703 (2023).
54. Brown, M. L. & Schneyer, A. L. Emerging roles for the TGFbeta family in pancreatic beta-cell homeostasis. *Trends Endocrinol. Metab.* **21**, 441–448 (2010).
55. Hansen, J. S. & Plomgaard, P. Circulating follistatin in relation to energy metabolism. *Mol. Cell Endocrinol.* **433**, 87–93 (2016).
56. Schneyer, A. L., Wang, Q., Sidis, Y. & Sluss, P. M. Differential distribution of follistatin isoforms: application of a new FS315-specific immunoassay. *J. Clin. Endocrinol. Metab.* **89**, 5067–5075 (2004).
57. Thompson, T. B., Lerch, T. F., Cook, R. W., Woodruff, T. K. & Jardetzky, T. S. The structure of the follistatin:activin complex reveals antagonism of both type I and type II receptor binding. *Dev. Cell* **9**, 535–543 (2005).
58. Amthor, H. et al. Follistatin regulates bone morphogenetic protein-7 (BMP-7) activity to stimulate embryonic muscle growth. *Dev. Biol.* **243**, 115–127 (2002).
59. Derynck, R. & Budi, E. H. Specificity, versatility, and control of TGF-beta family signaling. *Sci. Signal.* **12**, eaav5183 (2019).
60. Hansen, J. et al. Exercise induces a marked increase in plasma follistatin: evidence that follistatin is a contraction-induced hepatokine. *Endocrinology* **152**, 164–171 (2011).
61. Hansen, J. S. et al. Circulating follistatin is liver-derived and regulated by the glucagon-to-insulin ratio. *J. Clin. Endocrinol. Metab.* **101**, 550–560 (2016).
62. Singh, R. et al. Metabolic profiling of follistatin overexpression: a novel therapeutic strategy for metabolic diseases. *Diab. Metab. Syndr. Obes.* **11**, 65–84 (2018).
63. Lin, T. et al. Follistatin-controlled activin-HNF4alpha-coagulation factor axis in liver progenitor cells determines outcome of acute liver failure. *Hepatology* **75**, 322–337 (2022).
64. Wu, C. et al. Elevated circulating follistatin associates with an increased risk of type 2 diabetes. *Nat. Commun.* **12**, 6486 (2021).
65. Boland, M. L. et al. Towards a standard diet-induced and biopsy-confirmed mouse model of non-alcoholic steatohepatitis: Impact of dietary fat source. *World J. Gastroenterol.* **25**, 4904–4920 (2019).
66. Hansen, H. H. et al. Human translatability of the GAN diet-induced obese mouse model of non-alcoholic steatohepatitis. *BMC Gastroenterol.* **20**, 210 (2020).
67. Hansen, H. H. et al. Semaglutide reduces tumor burden in the GAN diet-induced obese and biopsy-confirmed mouse model of NASH-HCC with advanced fibrosis. *Sci. Rep.* **13**, 23056 (2023).
68. Neuschwander-Tetri, B. A. Therapeutic landscape for NAFLD in 2020. *Gastroenterology* **158**, 1984–1998 (2020).
69. Kristiansen, M. N. et al. Obese diet-induced mouse models of nonalcoholic steatohepatitis-tracking disease by liver biopsy. *World J. Hepatol.* **8**, 673–684 (2016).
70. Van Herck, M. A., Vonghia, L. & Francque, S. M. Animal models of nonalcoholic fatty liver disease-a starter's guide. *Nutrients* **9**, 1072 (2017).
71. Maher, J. J., Leon, P. & Ryan, J. C. Beyond insulin resistance: Innate immunity in nonalcoholic steatohepatitis. *Hepatology* **48**, 670–678 (2008).
72. Li, P. et al. Hematopoietic-derived galectin-3 causes cellular and systemic insulin resistance. *Cell* **167**, 973–984 e912 (2016).
73. Li, H. et al. Chronic high-fat diet induces galectin-3 and TLR4 to activate NLRP3 inflammasome in NASH. *J. Nutritional Biochem.* **112**, 109217 (2023).
74. Ishimoto, T. et al. High-fat and high-sucrose (western) diet induces steatohepatitis that is dependent on fructokinase. *Hepatology* **58**, 1632–1643 (2013).
75. Vos, M. B. & Lavine, J. E. Dietary fructose in nonalcoholic fatty liver disease. *Hepatology* **57**, 2525–2531 (2013).
76. Haas, J. T. et al. Hepatic insulin signaling is required for obesity-dependent expression of SREBP-1c mRNA but not for feeding-dependent expression. *Cell Metab.* **15**, 873–884 (2012).
77. Arrese, M., Cabrera, D., Kalergis, A. M. & Feldstein, A. E. Innate immunity and Inflammation in NAFLD/NASH. *Dig. Dis. Sci.* **61**, 1294–1303 (2016).
78. Febbraio, M. A. & Karin, M. Sweet death": Fructose as a metabolic toxin that targets the gut-liver axis. *Cell Metab.* **33**, 2316–2328 (2021).
79. Xu, R., Tao, A., Zhang, S. & Zhang, M. Neutralization of interleukin-17 attenuates high fat diet-induced non-alcoholic fatty liver disease in mice. *Acta Biochim Biophys. Sin. (Shanghai)* **45**, 726–733 (2013).
80. Kazankov, K. et al. The role of macrophages in nonalcoholic fatty liver disease and nonalcoholic steatohepatitis. *Nat. Rev. Gastroenterol. Hepatol.* **16**, 145–159 (2019).
81. Smith, G. I. et al. Insulin resistance drives hepatic de novo lipogenesis in nonalcoholic fatty liver disease. *J. Clin. Investig.* **130**, 1453–1460 (2020).
82. Ortega-Prieto, P. & Postic, C. Carbohydrate sensing through the transcription factor ChREBP. *Front. Genet.* **10**, 472 (2019).
83. Herman, M. A. & Birnbaum, M. J. Molecular aspects of fructose metabolism and metabolic disease. *Cell Metab.* **33**, 2329–2354 (2021).
84. Duarte, J. A. et al. A high-fat diet suppresses de novo lipogenesis and desaturation but not elongation and triglyceride synthesis in mice. *J. Lipid Res.* **55**, 2541–2553 (2014).
85. Zhao, S. et al. Dietary fructose feeds hepatic lipogenesis via microbiota-derived acetate. *Nature* **579**, 586–591 (2020).
86. Roumans, K. H. M. et al. Hepatic saturated fatty acid fraction is associated with de novo lipogenesis and hepatic insulin resistance. *Nat. Commun.* **11**, 1891 (2020).
87. Andres-Hernando, A. et al. Deletion of fructokinase in the liver or in the intestine reveals differential effects on sugar-induced metabolic dysfunction. *Cell Metab.* **32**, 117–127(2020).
88. Devarbhavi, H. et al. Global burden of liver disease: 2023 update. *J. Hepatol.* **79**, 516–537 (2023).
89. Radhakrishnan, S., Yeung, S. F., Ke, J. Y., Antunes, M. M. & Pellizzon, M. A. Considerations when choosing high-fat, high-fructose, and high-cholesterol diets to induce experimental nonalcoholic fatty liver disease in laboratory animal models. *Curr. Dev. Nutr.* **5**, nzab138 (2021).
90. Guo, S. et al. The Irs1 branch of the insulin signaling cascade plays a dominant role in hepatic nutrient homeostasis. *Mol. Cell Biol.* **29**, 5070–5083 (2009).

91. Petersen, M. C. et al. Insulin receptor Thr1160 phosphorylation mediates lipid-induced hepatic insulin resistance. *J. Clin. Investig.* **126**, 4361–4371 (2016).
92. Summers, S. A. & Goodpaster, B. H. CrossTalk proposal: Intramyocellular ceramide accumulation does modulate insulin resistance. *J. Physiol.* **594**, 3167–3170 (2016).
93. Cheng, Z. et al. Foxo1 integrates insulin signaling with mitochondrial function in the liver. *Nat. Med.* **15**, 1307–1311 (2009).
94. Jang, C. et al. The Small intestine converts dietary fructose into glucose and organic acids. *Cell Metab.* **27**, 351–361 e353 (2018).
95. Guillot, A. & Tacke, F. Liver Macrophages: old dogmas and new insights. *Hepatol. Commun.* **3**, 730–743 (2019).
96. Hammerich, L. & Tacke, F. Hepatic inflammatory responses in liver fibrosis. *Nat. Rev. Gastroenterol. Hepatol.* **20**, 633–646 (2023).
97. Febbraio, M. A. et al. Preclinical models for studying NASH-driven HCC: how useful are they?. *Cell Metab.* **29**, 18–26 (2019).
98. Todoric, J. et al. Fructose stimulated de novo lipogenesis is promoted by inflammation. *Nat. Metab.* **2**, 1034–1045 (2020).
99. Verbeek, J. et al. Roux-en-y gastric bypass attenuates hepatic mitochondrial dysfunction in mice with non-alcoholic steatohepatitis. *Gut.* **64**, 673–683 (2015).
100. Beringer, A. & Miossec, P. IL-17 and IL-17-producing cells and liver diseases, with focus on autoimmune liver diseases. *Autoimmun. Rev.* **17**, 1176–1185 (2018).
101. Stohr, O., Tao, R., Miao, J., Copps, K. D. & White, M. F. FoxO1 suppresses Fgf21 during hepatic insulin resistance to impair peripheral glucose utilization and acute cold tolerance. *Cell Rep.* **34**, 16 (2021).
102. Wattacheril, J. & Sanyal, A. J. Lean NAFLD: an underrecognized outlier. *Curr. Hepatol. Rep.* **15**, 134–139 (2016).
103. Klein, R. J., Viana Rodriguez, G. M., Rotman, Y. & Brown, R. J. Divergent pathways of liver fat accumulation, oxidation, and secretion in lipodystrophy versus obesity-associated NAFLD. *Liver Int* **43**, 2692–2700 (2023).
104. Tao, R. et al. Hepatic FoxOs regulate lipid metabolism via modulation of expression of the nicotinamide phosphoribosyltransferase gene. *J. Biol. Chem.* **286**, 14681–14690 (2011).

Acknowledgements

We thank Dr. M. Matzuk for providing the $Fst^{L/L}$ mice and Dr. R. DePinho for providing the $FoxO1^{L/L}$ mice. This work was supported by NIH grants DK137942 (M.F.W.), DK098655 (M.F.W.), AG067913 (M.F.W.), DK133388 (R.T.), DK108859 (M.A.L.), and grants to Ji Miao (DK124328, DK133331).

Author contributions

M.F.W. and R.T. designed the research direction and analyzed all the data. The manuscript was written by R.T., K.D.C., and M.F.W. R.T. performed most of the experiments with collaboration from K.D.C. N.S. analyzed data from the Tübingen Diabetes Family Study (TDFS). M.A.L and A.A.-H. provided $Khk^{L/L}$ mice. O.S., W.Q., B.H., and C.W. provided technical support. L.G. conducted the RNAseq. O.T. and H.S. conducted the [^{13}C]fructose tracing, and C.B. provided the LC-MS analysis of TAG species in liver extracts.

Competing interests

The authors declare the following competing interests: M.F.W. is a scientific consultant for Housey Pharmaceutical Research Laboratories; M.A.L. is a member of Colorado Research Partners (CRP). Other authors declare no competing interests, including R.T., O.S., O.T., A.A.-H., W.Q., B.H., C.W., L.G., C.B., S.H., N.S., and K.D.C.

Additional information

Supplementary information The online version contains supplementary material available at https://doi.org/10.1038/s41467-025-66296-5.

Correspondence and requests for materials should be addressed to Morris F. White.

Peer review information *Nature Communications* thanks Sunhee Jung and the other, anonymous, reviewer(s) for their contribution to the peer review of this work. A peer review file is available.